RESEARCH TRIANGLE INSTITUTE

ASPECTS OF GULF STREAM WESTERN BOUNDARY EDDIES FROM SATELLITE AND IN SITU DATA

Final Report

Contract No. 7-35182

Prepared for

National Environmental Satellite Services
National Oceanic and Atmospheric Administration
Washington, D.C.

By

Fred M. Vukovich

and

Bobby W. Crissman

Research Triangle Institute
Research Triangle Park
North Carolina 27709

May 1979

RESEARCH TRIANGLE PARK, NORTH CAROLINA 27709

Aspects of Gulf Stream Western Boundary Eddies from Satellite and In Situ Data

Final Report

Contract No. 7-35182

Prepared for

National Environmental Satellite Service
National Oceanic and Atmospheric Administration
Washington, D.C.

By

Fred M. Vukovich

and

Bobby W. Crissman

Research Triangle Institute
Research Triangle Park
North Carolina 27709

May 1979

ABSTRACT

NOAA-5 infrared imagery were used to determine statistics of existing and developing eddies on the western boundary of the Gulf Stream. The satellite data were then combined with in situ data to study the physics and dynamics of both a new-born eddy and one which had been in existance for a considerable time. A simple linear model of flow over a topographic feature similar to the Charleston Bump was developed.

The results of the study showed that, on the average, the perturbations are much more intense, have larger dimensions, and move slower when they are located immediately downstream of the Charleston Bump, a region where the bottom topography is influenced by the Blake Plateau, than when the eddies were located farther downstream in a region where the slope is steep. The results of the theoretical model compare well with observed data, suggesting that the perturbations may indeed be lee waves.

TABLE OF CONTENTS

LIST OF FIGURES

LIST OF FIGURES (continued)

LIST OF FIGURES (continued)

LIST OF TABLES

ACKNOWLEDGMENTS

The authors wish to acknowledge the interest and assistance of Dr. Richard Legeckis (contract monitor), and Dr. A. E. Strong of NOAA/NESS. The authors would also like to express their appreciation to Mr. John Pritchard (NOAA/NESS) for providing VHRR imagery and digital VHRR data for this research project; and they also wish to express their appreciation to the National Aeronautics and Space Administration, Langley Research Center, for providing the free drifting buoys for this experiment and to Captain Arthur Jordan, his staff, and the crew of the Cape Fear Technical Institute's R/V Northstar. We also would like to thank the numerous members of the NOAA weather station at the Raleigh/Durham Airport for their assistance in providing weather reports and collecting orbital data for the NOAA satellite.

The authors were assisted by Mr. J. W. Dunn (RTI) in the development of the computer algorithm for the analysis of the satellite sea-surface temperature data, by Ms. Dawn Erlich (RTI) in the analysis of the in situ data, and Mr. Mark Bushnell (formerly of RTI and presently of NOAA/AOML) in the analysis of the in situ data and the computations of vorticity from the model.

1.0 INTRODUCTION

Since the launch of the NOAA-1 satellite in 1970, the infrared images from the NOAA satellites have produced a significant body of data, indicating the existence of wavelike features along the western boundary of the Gulf Stream downstream of 32°N (the approximate latitude of Charleston, South Carolina). The initial observation of these perturbations was presented by Rao, Strong, and Koffler (1971). They detected a perturbation with a wavelength of approximately 197 km and an amplitude of about 86 km in March 1971. Later, DeRycke and Rao (1973) reported on a similar wave-type perturbation using NOAA-2 data. The perturbation was observed in April 1973 and had a wavelength of approximately 189 km and an amplitude of 73 km.

Stumpf and Rao (1975) presented data showing the evolution of the wavelike perturbations into eddies using NOAA-2 data. Their data showed that in a period of less than 3 days, perturbations off the southeast coast of the United States between Cape Romain and Cape Hatteras evolved into three distinct regions of alternating cold and warm tongues. These tongues strongly suggested cyclonic motion. The transition may be due to either strong northwesterly surface winds, topographic influences of the coast line and continental margin, or baroclinic and/or baratropic instability associated with the Gulf Stream, shelf-water interface, or a combination of these factors.

Vukovich and Crissman (1975) used satellite and hydrographic data to show that, in some cases, it is possible that these eddies may be due to the steering of currents on the shelf toward the Gulf Stream boundary by the shoals off the various capes from Cape Hatteras southward. This can lead to the penetration of a tongue of cold shelf water into the Gulf Stream. It

appeared that the shelf currents were wind driven since these effects took place immediately after a cold frontal passage. Their results suggested that the evolution of wavelike perturbations into alternating tongues of cold and warm water may be due, for the most part, to wind-driven effects on the shelf. All three perturbations observed by DeRycke and Rao occurred east of one of the three bays that exist between Cape Hatteras and Cape Romain. There is a shoal off each of the Capes, but that at Cape Romain is not as significant as that off the Capes to the north.

Legeckis (1979) presented a descriptive study of the wavelike perturbations north of 31°N. He indicated that these perturbations generally develop immediately downstream of a bottom feature known as the "Charleston Bump." He grouped his observations into five typical cases. In the deflection case (Case 1), the western boundary of the Gulf Stream, as defined by the sea-surface temperature, was deflected seaward at the Charleston Bump and then landward with no apparent wave motion downstream at least as far as Cape Hatteras. In the case of deflection with cyclonic rotation (Case 2), the western boundary was deflected seaward at the Charleston Bump and then appeared to rotate in a cyclonic sense. There was no significant wave motion apparent downstream at least as far as Cape Hatteras. In the third case (Case 3), the deflection appeared to move downstream. In the fourth case (Case 4), a wave train of stable waves appeared downstream of the Charleston Bump. The waves were called stable mainly because they resembled a combination of sinusoids and did not display cyclonic rotation. The last case (Case 5) was the unstable wave case and was identical to the situation described by DeRycke and Rao.

It has been suggested that the waves observed in the infrared images are thermal manifestations of continental shelf waves. In the presence of a sheared mean current (such as the Gulf Stream), continental shelf waves will propogate downstream (Niiler and Mysak, 1971, and Brooks, 1975) similar to what has been observed for these western boundary eddies. Shelf waves can be produced by barotropic and/or baroclinic instabilities. Orlanski (1969) used a two-layer model of the Gulf Stream and found that the continental rise can produce baroclinic instabilities, resulting in downstream propogating waves with wavelengths on the order of 200 km and a period of about 10 days. Niiler and Mysak found unstable waves of 150- to 200-km wavelengths belonging to a class of barotropic instabilities. The period depended on the local topography and ranged for an eastern continental shelf from about 10 to 21 days for the fastest growing waves.

Mysak and Hamon (1969) performed a statistical analysis of the semi-diurnal mean fluctuation of sea level and of atmospheric pressure from data obtained at the North Carolina coast. They found that the response of sea level to pressure was nonbarometric, especially in the period of 3 to 10 days. They found evidence of upstream propagation of the waves, which is in contrast to the downstream propagation of the waves found in the satellite data.

Schott and Düing (1976) studied current measurements from three stations off the east coast of Florida, and found significant results in the 10- to 13-day band and near significant results in the 7- to 10-day band. The wavelengths were about 170 km and they propogated upstream. About 70 percent of the measured kinetic energy was due to a barotropic wave, and the rest was incoherent. The 10- to 13-day band agreed rather well with model calculation by Brooks (1975).

In this study, the NOAA-5 VHRR data were used to glean statistics on the wavelength, amplitude, and speed of the waves found between 32°N and 36°N, and to describe the development of a perturbation immediately downstream of the Charleston Bump. In the spring of 1977, the Research Triangle Institute (RTI), in cooperation with the Cape Fear Technical Institute (CFTI), performed a series of real-time oceanographic studies. Infrared images obtained by the RTI satellite receiving station (RTI/SRS) from the NOAA-5 satellite were used to detect and locate the western boundary eddies, and to plan an oceanic field program. A ship from CFTI was dispatched into the region of interest to collect in situ data and to launch one or more satellite-tracked, free-drifting buoys within the eddy. The buoys were located by the Random Access Measurement Systems (RAMS) aboard the NIMBUS-6 satellite. The results of this study are also presented. Lastly, a simple linear theory is presented which suggests that flow over topographic features such as the Charleston Bump may be sufficient to produce cyclonic perturbations such as that observed in the IR imagery.

2.0 SATELLITE DATA AND SHIP DATA

2.1 NOAA Satellite Data

The NOAA-5 satellite was launched in near polar orbit on 29 July 1976. The satellite is equipped with two radiometers capable of detecting surface temperature. The Scanning Radiometer (SR) detects radiation in the 10- to 12.5-μm infrared water vapor window. Aspects of the absorption characteristic of this band have been discussed by Vukovich and Blanton (1969), Kunde (1965), Smith et al. (1970), and Vukovich (1972). The SR, a medium resolution radiometer, has a surface resolution of 7.5 km at nadir (0° angle) at the satellite's operating altitude of approximately 1,500 km.

The IR data are transmitted to ground stations in analog form and in one of two modes. Most of the data collected during one orbit are stored on tape recorders aboard the satellite and are transmitted at some later time to a NOAA ground acquisition station. Selected data are digitized, converted into black-body temperatures, rectified in space, and stored for later use.

Direct readout data are also available from the SR using the Automatic Picture Transmission (APT) service provided by these satellites. Data are received only when the satellite is in the range of a ground station. The APT data were received by the RTI/SRS (for details on the RTI/SRS, see Vukovich and Crissman, 1977), and were used to detect and locate oceanic perturbations and to design an oceanic field program. Rectification of the APT data was done subjectively, based on available landmarks.

The Very High Resolution Radiometer (VHRR) data are also available from the NOAA-5 satellite. This radiometer detects IR radiations in the same water vapor window band as does the SR, but the VHRR has better resolution.

The ground resolution is 0.9 km at nadir at a satellite altitude of 1,500 km. The data are transmitted directly to a NOAA ground acquisition station as a part of the High Resolution Picture Transmission (HRPT) service.

The VHRR data, because of the superior resolution, were used to establish the sea-surface temperature patterns associated with the western boundary eddies in the analysis phase of this study. Two modes of data were provided by the National Environmental Satellite Service (NESS). One mode was infrared images, which were specially enhanced and processed to have all distances linear. The other mode was digital data, which were used to determine the sea-surface distribution in the perturbation.

2.2 NIMBUS-6 Data

As a part of this experiment, satellite-tracked, free-drifting buoys were launched within the western boundary eddies. The position of the buoys was monitored by the NIMBUS-6 Random Access Measurements System (RAMS) (see NIMBUS-6 Users Guide, 1975). Successive positions of the buoys yielded an estimate of the trajectory of a water parcel at approximately the 3-m depth, since the buoys' "sea anchor" was set at that level.

Each buoy transmits a Doppler signal at a carrier frequency of 401.2 mHz. These signals are transmitted to space for 1 second of each minute. When the NIMBUS-6 satellite is in the near proximity of the buoy, the platform signals were detected, demodulated, and stored. Processing of the Doppler signals on the ground provides the position and velocity of each buoy. Expected positioning error is ± 2.0 km.

2.3 Ship Data

After the RTI/SRS was used to obtain the APT data and a western boundary was detected and located in space, an oceanic field program was designed to gather hydrographic data within the perturbation. Usually, within 24

hours, a ship was dispatched from CFTI in Wilmington, North Carolina. For the particular studies described in this report, the R/V North Star was employed to perform the data collection. Surface temperatures were obtained by towing a thermister at the surface; subsurface temperature and salinity data were collected by a Salinity, Temperature, and Depth (STD) instrument at various stations along specified transects. Subsurface data were obtained to the 500-m depth or to the bottom if the depth was less than 500 m. Calibration of instruments was performed before and after the study period. As indicated earlier, at specific locations determined from the analysis of the APT images, free-drifting buoys were launched within the perturbation in order to obtain some estimates of circulation.

3.0 STATISTICS ON WESTERN BOUNDARY EDDIES

3.1 Procedure

The NOAA-5 VHRR images for the period January through May 1977 were analyzed for western boundary eddies in the region 32°N northward to 36°N. The latitude 32°N is the approximate latitude of the Charleston Bump. The 200-m topographic contour was used to locate the position of a shelf break for this analysis. When a western boundary eddy was noted, the image was gridded, the thermal boundaries of the perturbation were located in space (latitude and longitude coordinates), and the feature was transferred to a scaled map of the region of interest. Because the perturbations were near the coast, it is estimated that there was, at most, a ± 10-km error in gridding the satellite images and transferring features to scaled maps. The analyses of the scaled maps were used to develop statistics on the perturbations.

There were, on the average, about 3 days between clear sky images, and about three observations of each eddy. This allowed for three separate appraisals of static measurements (e.g., wavelength and amplitude) and about two separate time-dependent measurements (e.g., wave speed). Based on the estimated gridding error of ± 10 km, wave speed errors can range from 0 to ± 6 km day^{-1} with an average error of ± 3 km day^{-1}. For this analysis, the wave speed was assumed to be equal to the product of the wave frequency and wavelength. The wave period was calculated through this formulation.

The primary parameters for which statistics were derived were wavelength, amplitude and wave speed. In order to obtain the wavelength and amplitude, a "best fit" sine curve was matched with the thermal manifestation of the eddy on scaled maps, and the wavelength (L) and amplitude (A)

were determined as defined in Figure 1. The wave speed was determined by noting successive positions of the wave crest. Best estimates were accomplished when crest positions were established from satellite imagery obtained at least 2 days apart.

3.2 Results

Figure 2 presents frequency distributions for wavelength, amplitude, and wave speed of the eddies observed over the period. In each figure, frequency distributions are presented for all perturbations found in the region 32°N to 36°N (A), in the region 32°N to 34°N (B), and in the region 34°N to 36°N (C). The subdivisions (B) and (C) are presented because of incoherence in the statistics found in case (A) and because of the marked differences in the characteristics of the shelf in these two regions. North of 34°N, the shelf slope is considerably steeper than that south of 34°N. Table 1 summarizes the important information in the figures.

The data for case (A) indicates that the perturbations have an average wavelength of 139 km, an amplitude of 47 km, a downstream wave speed of 27 km day^{-1}, and a period of approximately 5 days. Legeckis (1979) examined essentially this same period and found that the average wavelength of about 150 km for these eddies. It is noted that there is little coherence between the average, medium, and mode, particularly for the wavelengths and period. This suggested that there may be perturbations of different characteristics within the total data set.

When the data set was divided into those perturbations found south of 34°N and those found north of 34°N, there was considerably more coherence in the statistics. On the average, the perturbations found south of 34°N (B) have a wavelength of approximately 148 km, an amplitude of 52 km, a downstream

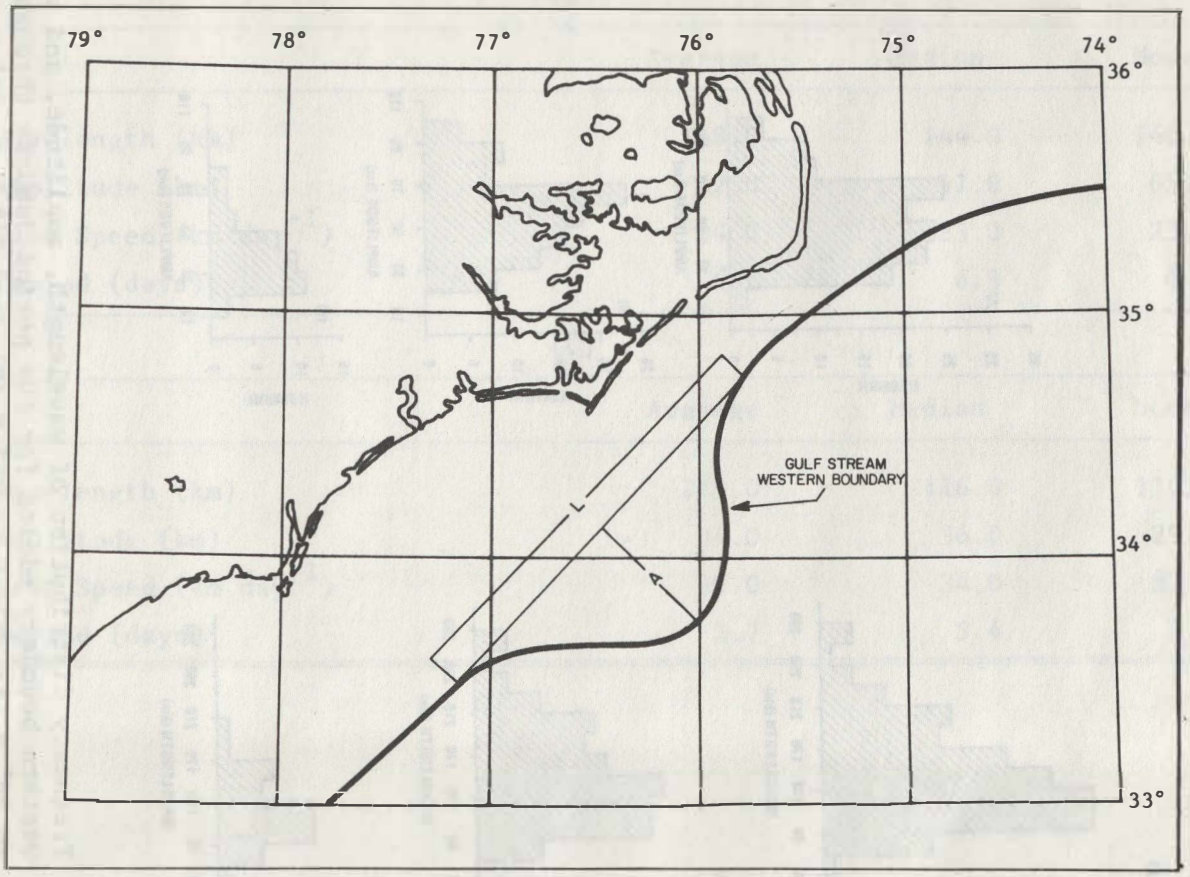

Figure 1. Graphical description of the parameters L (wavelength) and A (amplitude).

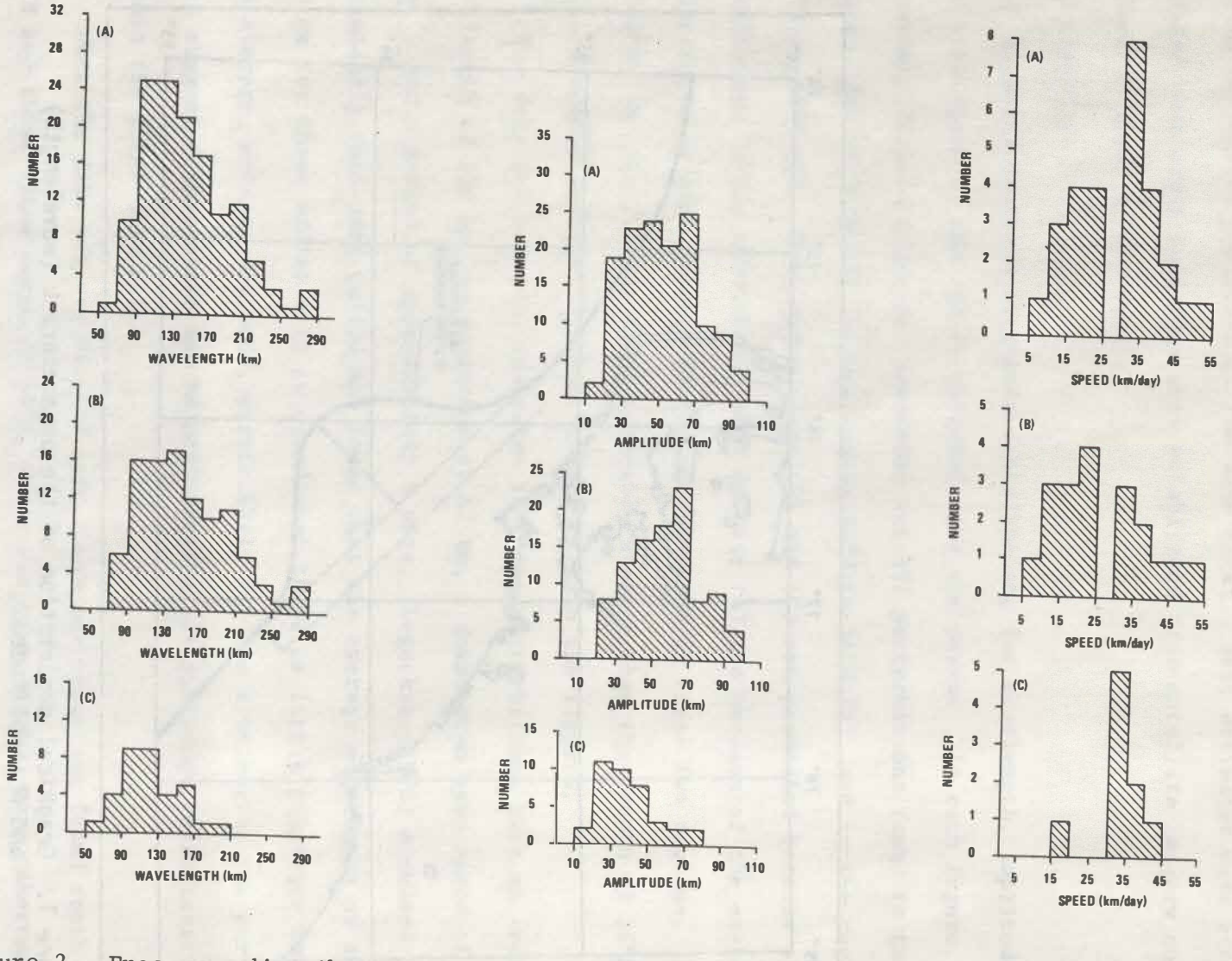

Figure 2. Frequency distribution of wavelength, amplitude, and wave speed of Gulf Stream western boundary eddies for the period January through May 1977 in the region 32° N to 36° N (A), 32° N to 34° N (B), and 34° N to 36° N (C).

TABLE 1. STATISTICS ON WAVE CHARACTERISTICS FOR WESTERN BOUNDARY EDDIES LOCATED (A) NORTH OF 32°N AND SOUTH OF 36°N, (B) NORTH OF 32°N AND SOUTH OF 34°N, AND (C) NORTH OF 34°N AND SOUTH OF 36°N, BASED ON DATA FOR JANUARY-MAY 1977

(A)

	Average	Median	Mode
Wavelength (km)	139.0	135.0	110.0
Amplitude (km)	47.0	50.0	65.0
Speed (km day^{-1})	27.0	33.0	33.0
Period (days)	5.2	4.1	3.3

(B)

	Average	Median	Mode
Wavelength (km)	148.0	144.0	140.0
Amplitude (km)	52.0	57.0	65.0
Wave Speed (km day^{-1})	24.0	23.0	23.0
Period (days)	6.2	6.3	6.1

(C)

	Average	Median	Mode
Wavelength (km)	115.0	116.0	110.0
Amplitude (km)	34.0	36.0	25.0
Wave Speed (km day^{-1})	31.0	34.0	33.0
Period (days)	3.7	3.4	3.3

wave speed of 24 km day^{-1}, and a period of approximately 6 days. North of 34°N, the average wavelength was approximately 115 km, the amplitude approximately 34 km, the downstream wave speed approximately 31 km day^{-1}, and the period approximately 4 days. The data indicate that perturbations are larger and move more slowly immediately downstream of the Charleston Bump, and are smaller but move faster farther downstream from the bump. The differences in the dimensions of the perturbations may reflect energy dispersion. The differences in speed may, in part, be due to the fact that in their formative stages, these waves, at times, become stationary.

4.0 TIME HISTORY OF EDDY DEVELOPMENTS

In the period 9 April through 15 April 1977, a remarkable sequence of VHRR images was obtained by the NOAA-5 satellite of a Gulf Stream western boundary eddy in its formative stages. The following is a descriptive analysis of the images obtained during that period. Table 2 gives various statistics gleaned from the satellite data on the eddy using the procedure described in Section 3.0.

Figure 3 is the NOAA-5 VHRR infrared image for 9 April 1977. Western boundary eddies are noted east of Onslow and Raleigh Bays. The feature of interest is the warm lens near the western boundary of the Gulf Stream east southeast of Cape Romain. This lens is separated from the Gulf Stream by a narrow zone of cold water. The first indication of the development of a western boundary eddy was seen in this precise location in the nighttime 10 April image (Figure 4). In the initial stages, the perturbation appeared as a cold tongue extending into the Gulf Stream. This cold tongue is located some 83 km downstream of the center of Charleston Bump in the precise position where the warm lens and narrow zone of cold water were located on the day before. An apparent warm tongue is located shoreward of the center of the cold tongue, giving the impression of cyclonic rotation. At this time, the wavelength of the perturbation is about 100 km and the amplitude, 30 km.

By the morning of 11 April (Figure 5), the infrared data indicated that the perturbation had grown (the wavelength is approximately 120 km and the amplitude, 40 km), and that the perturbation was moving downstream at a speed of approximately 26 km day^{-1}. The surface thermal pattern for the eddy is better defined and is in the form of cyclonically oriented, alter-

TABLE 2. STATISTICS ON THE WESTERN BOUNDARY EDDY DEVELOPING IN THE PERIOD 10 to 15 APRIL 1977

Date	Wavelength (km)	Amplitude (km)	Distance* (km)	Wave Speed ($km\ day^{-1}$)
10 April (night)	100	30	83	
11 April (morning)	120	40	96	26
11 April (night)	150	40	109	26
12 April (morning)	150	60	124	30
12 April (night)	160	60	148	48
13 April (morning)	160	60	167	30
13 April (night)	160	60	167	0
14 April (morning)	160	60	176	8
14 April (night)	160	60	185	18
15 April (morning)	160	60	213	56
15 April (night)	160	60	241	50

*This distance is the distance between the center of the eddy and the center of the Charleston Bump (~ 32°N and 79°W).

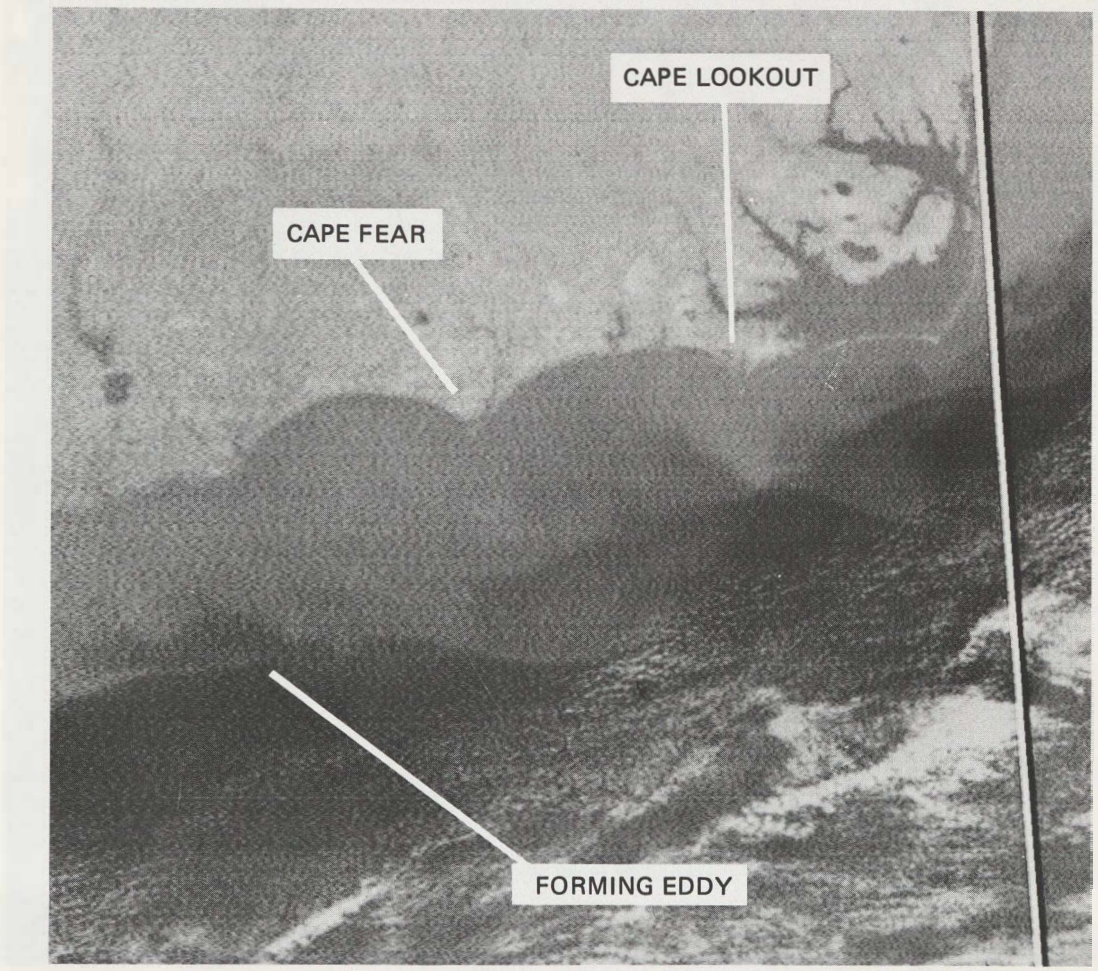

Figure 3. NOAA-5 infrared image for the night of 9 April 1977.

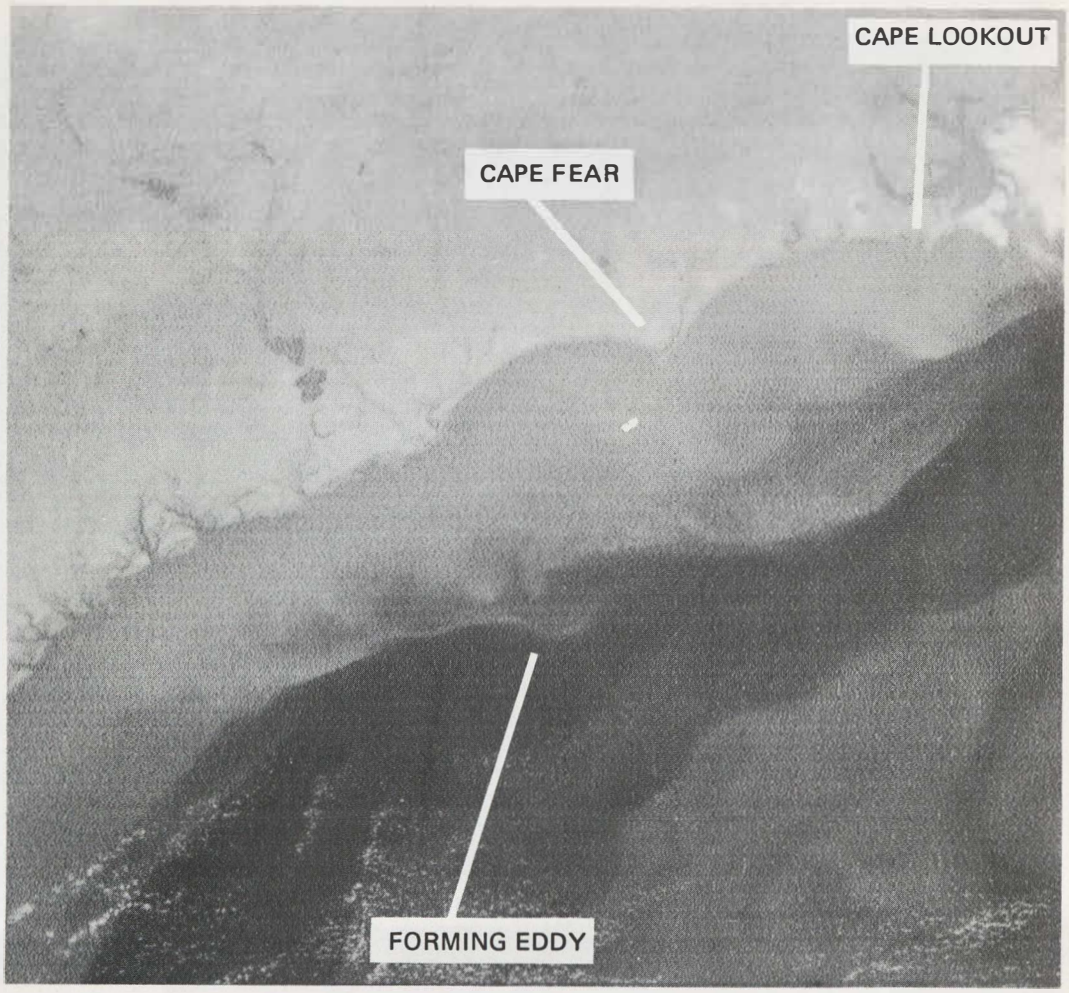

Figure 4. NOAA-5 infrared image for the night of 10 April 1977.

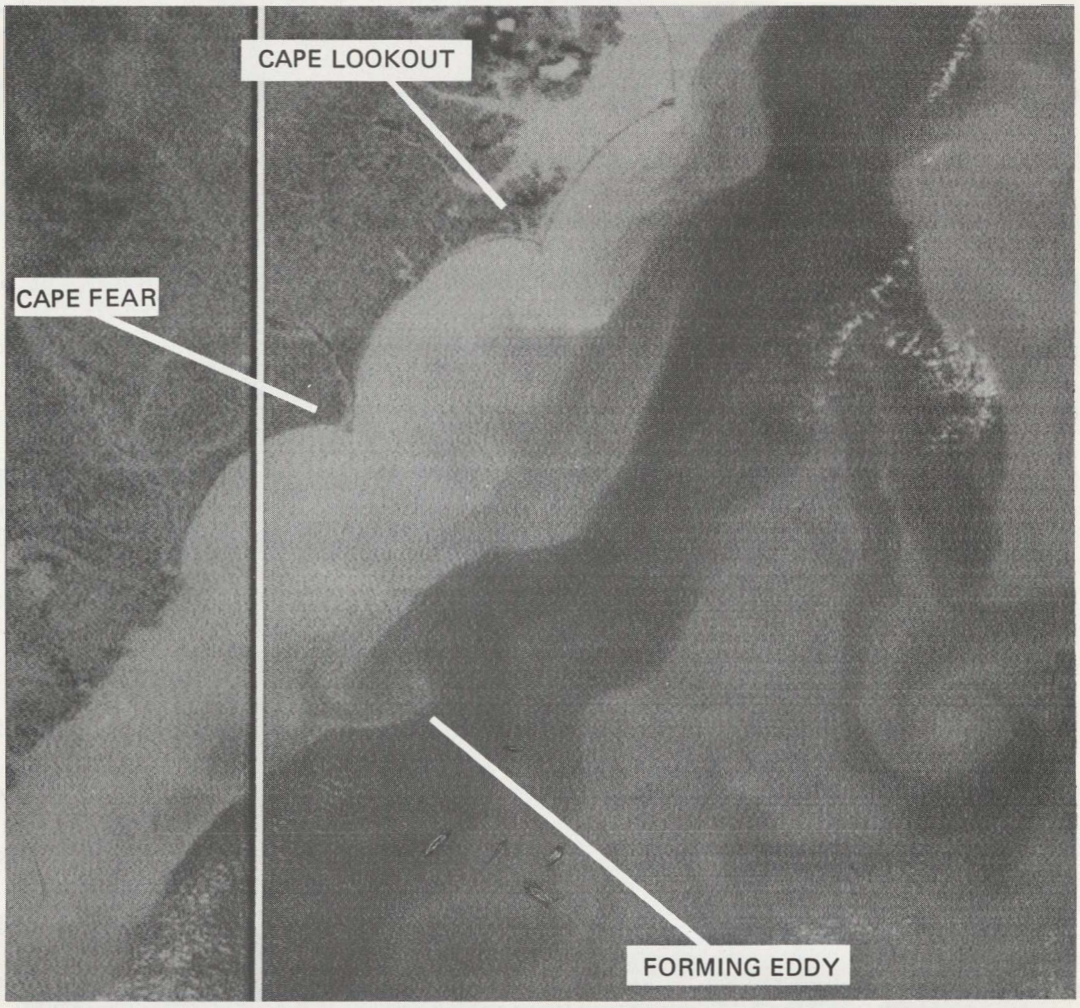

Figure 5. NOAA-5 infrared image for the morning of 11 April 1977.

nating cold and warm tongues, which supports the notion of cyclonic rotation. By the evening of 11 April (Figure 6), the perturbation had a wavelength of 150 km and an amplitude of 40 km and continued to move downstream at a speed of approximately 26 km day^{-1}.

On the morning of 12 April (Figure 7), the wavelength was about 150 km and the amplitude was 60 km. The perturbation continued to move downstream, but the speed of translation had increased to approximately 30 km day^{-1}. Though the image is obscured by scattered clouds in the region where the eddy is located, there are indications that the warm tongue is being circulated around the cold core of the eddy. The fact that the cold core is being sustained suggests that there may be upward vertical advection of cold subsurface water in the center of the eddy. This factor was much more evident in the nighttime image for 12 April (Figure 8). At this time, the eddy had a wavelength of 160 km and an amplitude of 60 km. The perturbation continued to move downstream and accelerated to a speed of 48 km day^{-1}. It is noted that the eddy appears to be a cold lens almost completely isolated from the shelf water.

There were no apparent changes in the wavelength and amplitude of the eddy after the night of 12 April to 15 April (the last day there was cloud-free imagery before a cold front moved in). There were changes in the wave speed, however. The perturbation was stationary on the night of 13 April; then accelerated, reaching a speed of 50 km day^{-1} by 15 April. The eddy took on characteristics of a wave by the morning of 14 April (Figure 9), and another eddy appeared to be forming upstream of the eddy of interest.

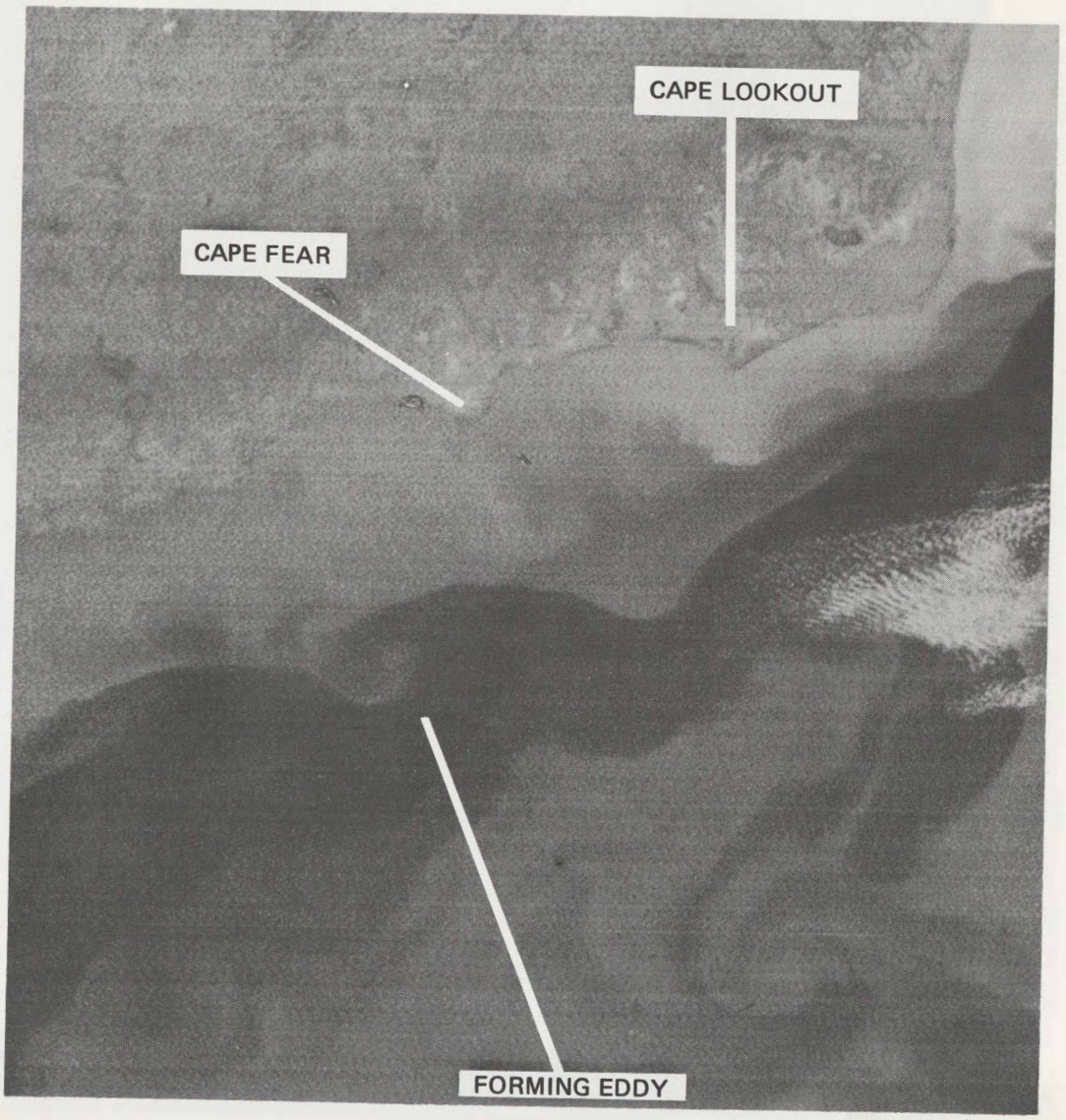

Figure 6. NOAA-5 infrared image for the night of 11 April 1977.

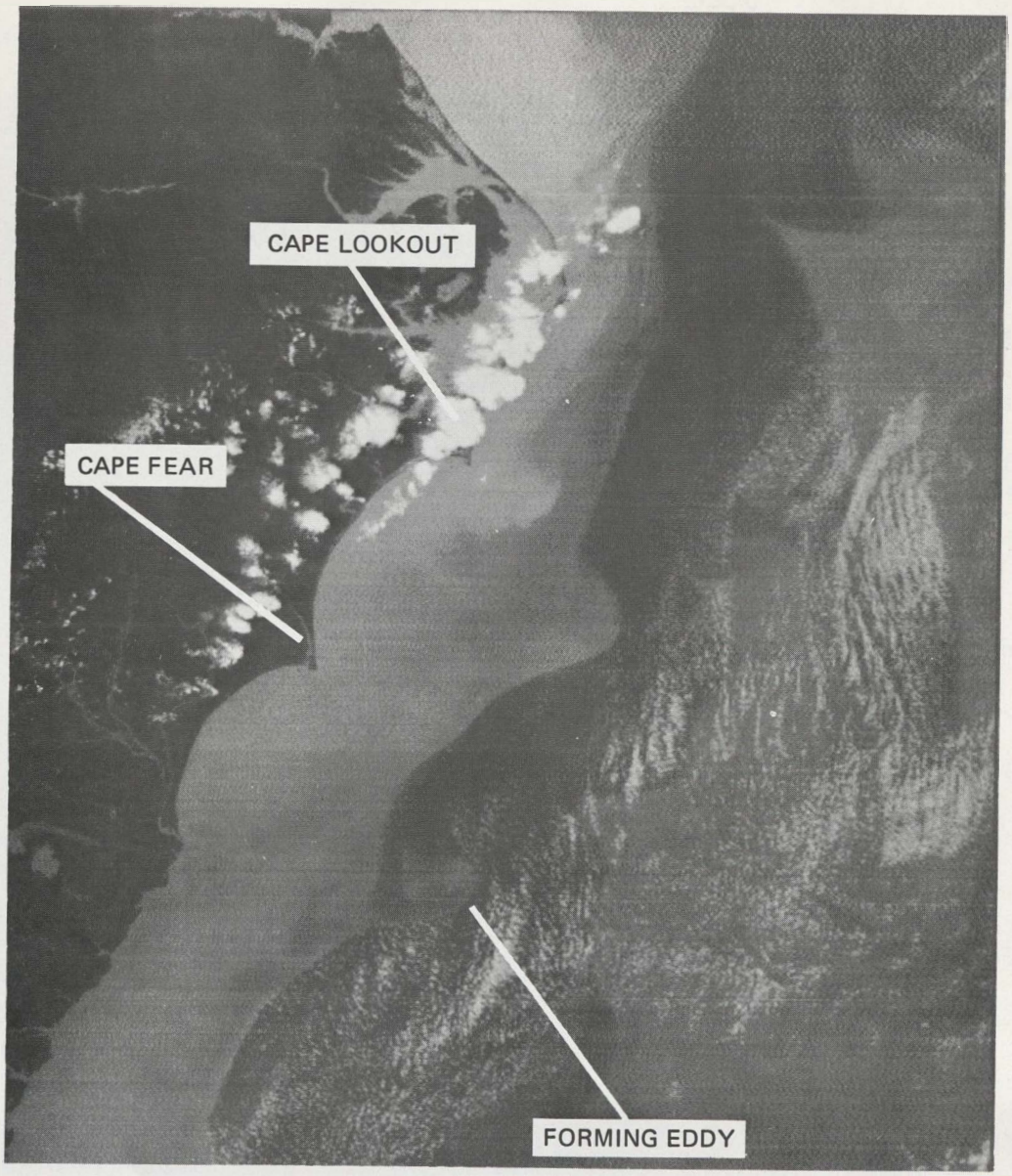

Figure 7. NOAA-5 infrared image for the morning of 12 April 1977.

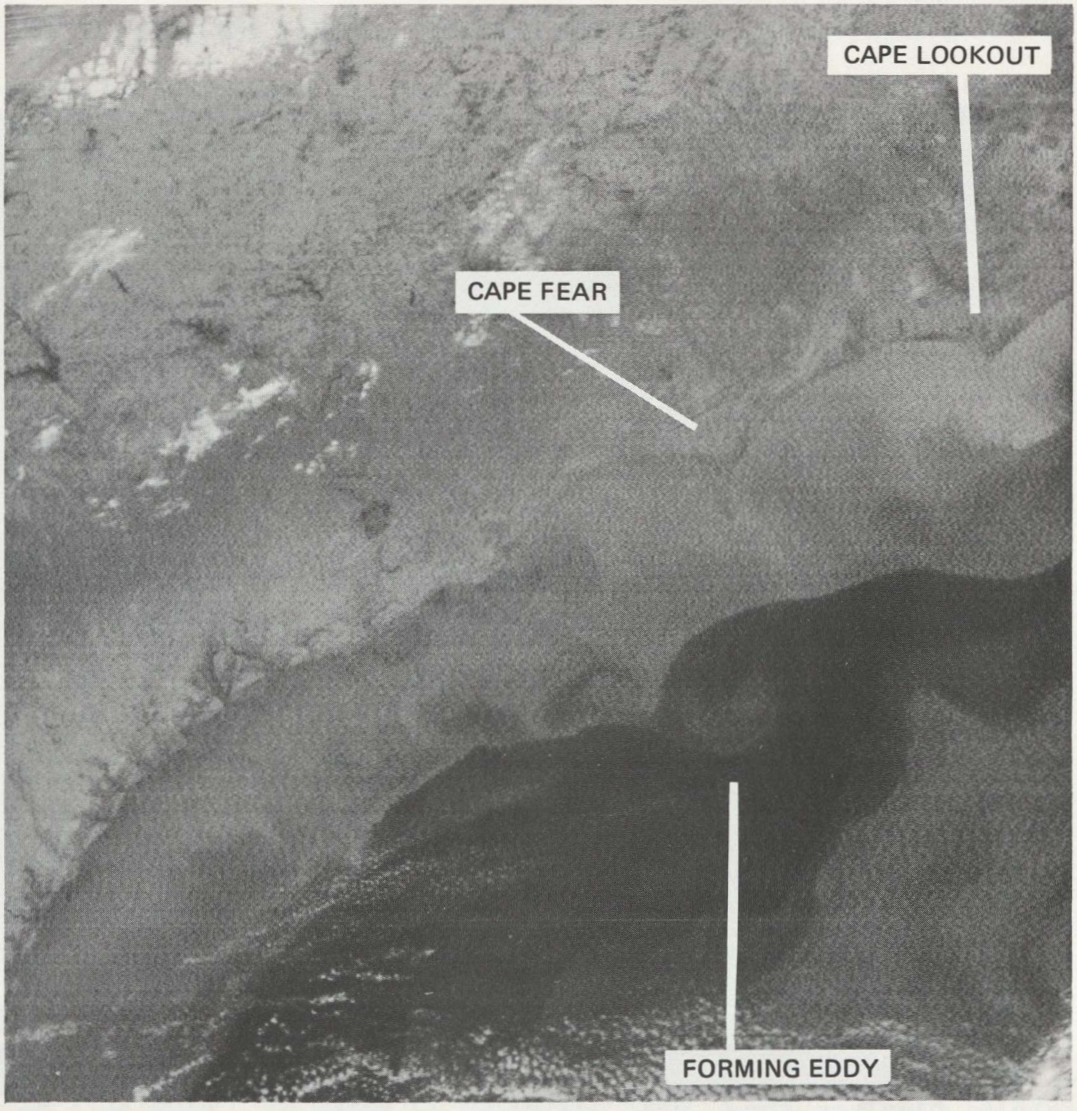

Figure 8. NOAA-5 infrared image for the night of 12 April 1977.

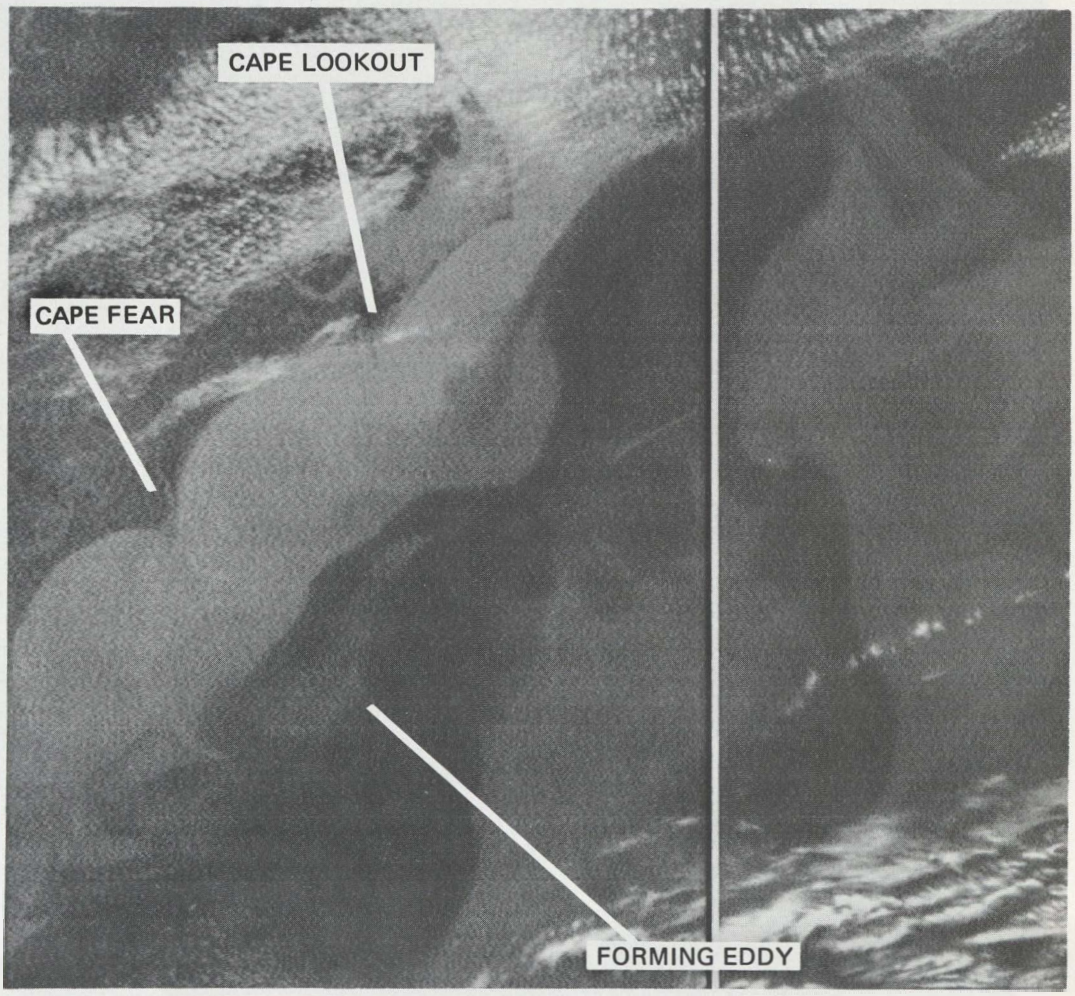

Figure 9. NOAA-5 infrared image for the morning of 14 April 1977.

5.0 CASE STUDIES

5.1 Introduction

This section presents the results of the analysis of the combined satellite and in situ data collected in western boundary eddies in the spring of 1977. Two case studies are presented. The first treats a newly formed western boundary eddy approximately 150 km downstream of the Charleston Bump. The second treats an eddy found approximately 330 km downstream of the bump east of Cape Lookout, North Carolina.

5.2 The 11 May 1977 Case Study

The first case treats a western boundary eddy formed sometime around 9 May 1977 and was well established by 11 May 1977. The in situ data collection was initiated based on the 9 May infrared image, and the data were collected during the period 11-14 May 1977. In this particular case, the eddy remained stationary for approximately 10 days and another field program was executed in the period 19-21 May 1977 in order to investigate the changes in the structure of the eddy with time. The eddy was located about 150 km northeast of the Charleston Bump in a region where the bottom topography is still influenced by the Blake Plateau.

5.2.1 Satellite Sea-Surface Temperature Analysis

Figure 10 is the sea-surface temperature analysis for 11 May 1977 obtained from digitized NOAA-5 infrared data. These data were received uncalibrated from NOAA. In order to calibrate them, a 1°C isotherm interval was established from the calibration curve obtained from the National Environmental Satellite Service. The value of the temperatures in the Gulf Stream were determined from the in situ data, and were used to determine the value of each isotherm in the analysis of the satellite data.

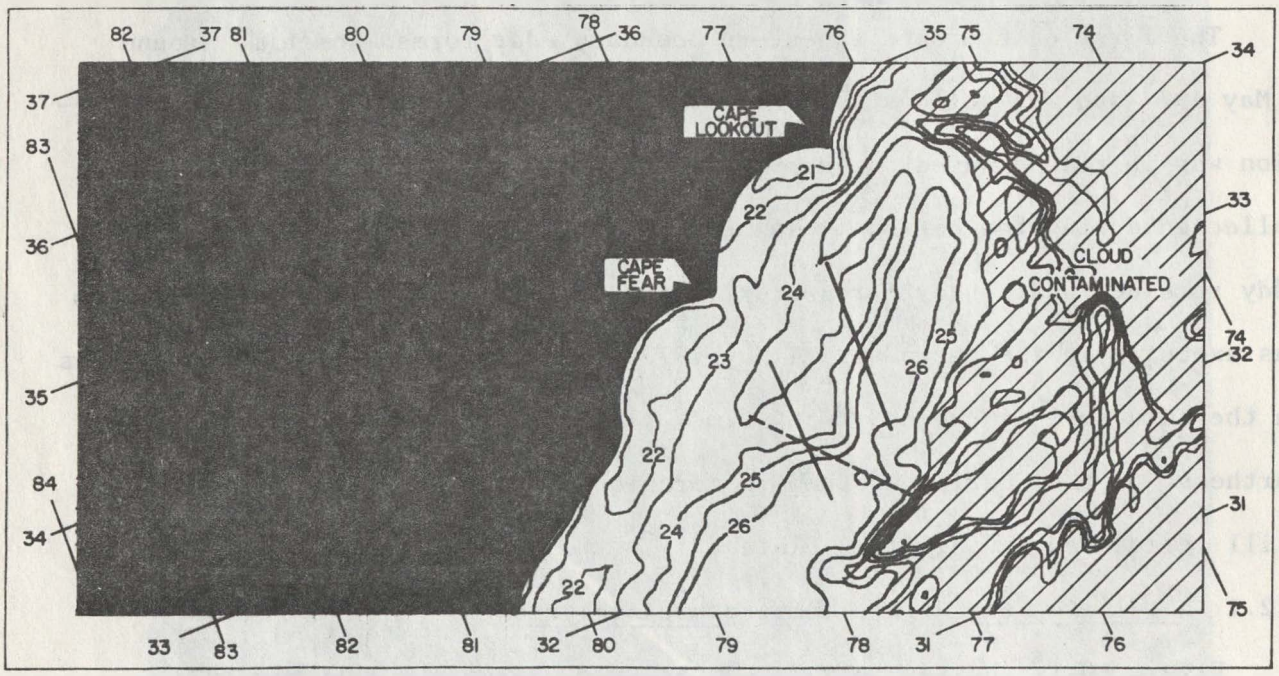

Figure 10. NOAA-5 sea-surface temperature (^{o}C) analysis for 11 May 1977.

Clouds contaminated the right-hand portion of the figure, but the region immediately off the coast of North Carolina and South Carolina had clearer skies. The water having temperatures greater than 26°C is the Gulf Stream. The temperatures off the coast in Raleigh Bay (the region immediately northeast of Cape Lookout) and Onslow Bay (the region immediately south of Cape Lookout) have temperatures on the order of 21°C to 22°C. The coastal region in Long Bay (the region immediately southwest of Cape Fear) has 22°C water. A western boundary eddy, having a wavelength of about 150 km, is noted east of Onslow Bay and Long Bay. The crest of the wave is located at approximately 77.5°W and 32.5°N. A cold tongue extends northward from the crest some 220 km, and a warm tongue originates immediately east of Cape Lookout (approximately 34.5°N), and extends some 220 km southwestward to 32.5°N.

The two solid lines shown in the figures are the transects performed during the 11-14 May field program. Transect 1 is located downstream (north) of the crest of the eddy along the 77°W longitude line from 34°N to 32.5°N. Transect 2 is found immediately upstream of the crest (south) along the 77.75°W longitude line from 32.25°N to 33.25°N. The dash line is a transect (Transect 3) obtained during the period 19-21 May, or approximately 7 days after Transect 2, and it is located in approximately the same position as Transect 2. The endpoints of Transect 3 are at 32°N and 77°W and 33°N and 78°W.

5.2.2 Subsurface Structure

Figure 11 shows the temperature, salinity, and density (σ_t) analyses from the data collected on Transect 1. The data were collected in the period 2315 EST on 11 May to 2122 EST on 12 May 1977. Eleven stations about 15 km apart were established along the transect.

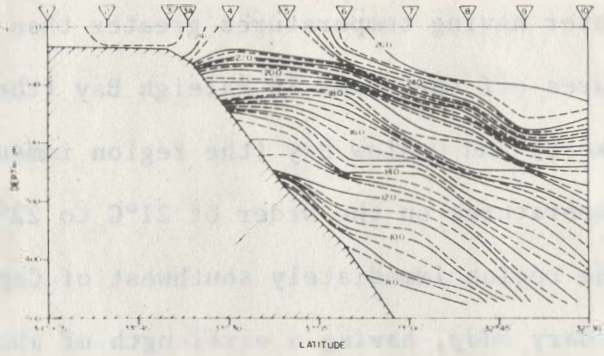

(A)

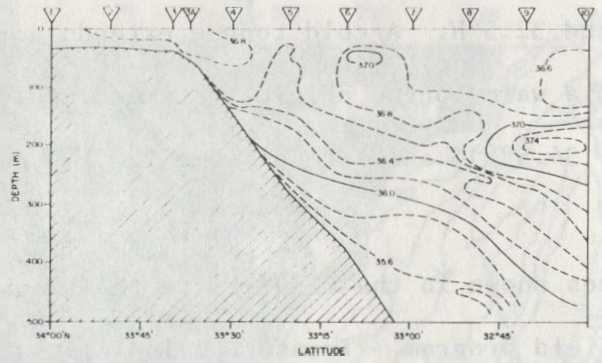

(B)

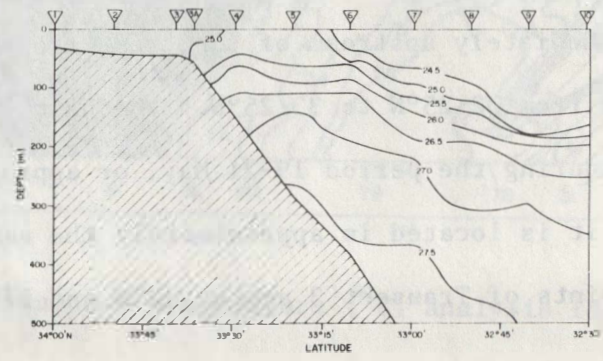

(C)

Figure 11. Cross-sectional analysis of (A) temperature (^{o}C), (B) salinity (‰), and (C) density (σ_t) along Transect 2.

The initial portion of this transect, esentially Stations 1-3a, were through the warm tongue associated with the western boundary eddy. This portion of the transect was on the shelf, and the analyses indicate that the shelf was characterized by warm, high-salinity, low-density water, extending from the surface to the shelf (approximately the 35-m depth). It is interesting to note that the salinity on the shelf in the surface layer is greater than that in the Gulf Stream in the surface layer (Stations 8 and 9). Immediately south of the warm tongue or where the transect intersected the cold tongue indicated in the satellite data, the surface layer (essentially the first 50 m) was characterized by cold, low-salinity, high-density water (i.e., compared to the water on the shelf). There is a temperature/density front associated with the Gulf Stream intersecting the surface between Stations 5 and 6. This front is weak compared to the intense subsurface front which intersects the shelf slope at about the 75-m depth. The temperature/density front is essentially horizontal in the subsurface across Stations 4 and 5 between the 75-m depth and the 150-m depth. Around the 300-m depth, there is cold, low-salinity, high-density water along the shelf slope.

The other interesting feature in the analysis is the tongue of high-salinity extending shoreward and upward from the high-salinity core of the Gulf Stream. The high-salinity core of the Gulf Stream is centered at around the 200-m depth between Stations 9 and 10. It would almost appear that if it was not for the dome of low salinity found at Station 5 between the surface and the 100-m depth, the high salinity on the shelf would be associated with that tongue of high salinity. The tongue is parallel to the temperature front which defines the Gulf Stream.

Figure 12 shows the temperature, salinity, and density analysis along Transect 2. Data were collected at seven stations approximately 15 km apart during the period 0348 EST to 1429 EST on 13 May 1977.

The transect did not extend sufficiently shoreward to describe in detail the nature of the water on the shelf. However, there are indications in the analyses, particular around Station 17, that there is warm, high-salinity water on the shelf. There was no indication of low-density water in that region, however.

A very intense Gulf Stream front is noted between the 50- and 75-m depth between Stations 13 and 17. In this region the front is practically horizontal with the vertical temperature gradient across the front of a 5.5°C in 25 m. The front intersects the shelf slope at about the 75-m depth. In comparison, a weak Gulf Stream front is noted at the surface (a temperature gradient of approximately 3.5°C in 55 km). The horizontal characteristic of the front between Stations 13 and 17 suggest that there may have been an override of low-density shelf water in the surface layer.

The most prominent feature in the analysis is the lens of cold, low-salinity, high-density water on the shelf slope centered at about the 325-m depth. This feature is located in the approximate position where the thermal wave was found at the surface using the satellite data. There is a dome of cold, low-salinity, high-density water projecting toward the surface from the lens.

Figure 13 shows the horizontal analyses of the temperature and salinity data from Transects 1 and 2 at the 100- and 300-m depths. The lens and dome appear to be directly associated with the thermal wave at the surface in Figure 11, and the scale of the feature in the *in situ* data appears to be

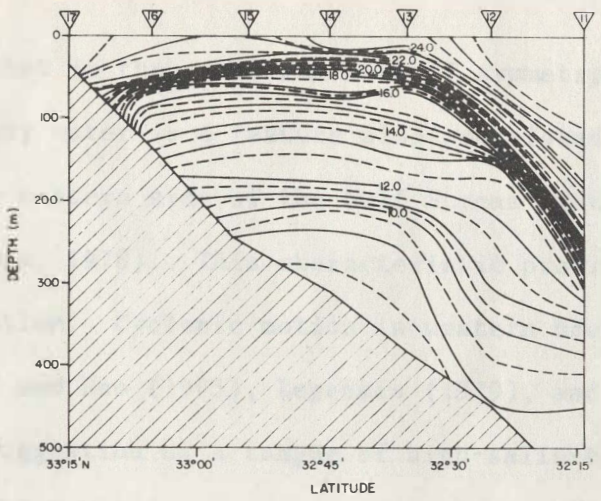

(A)

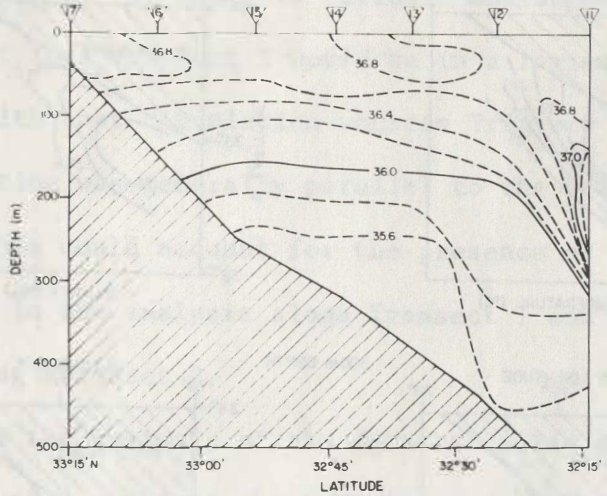

(B)

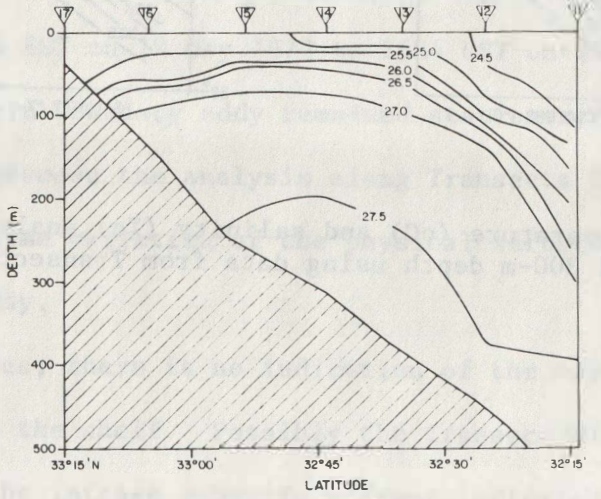

(C)

Figure 12. Cross-sectional analysis of (A) temperature (^{o}C), (B) salinity (‰), and (C) density (σ_t) along Transect 2.

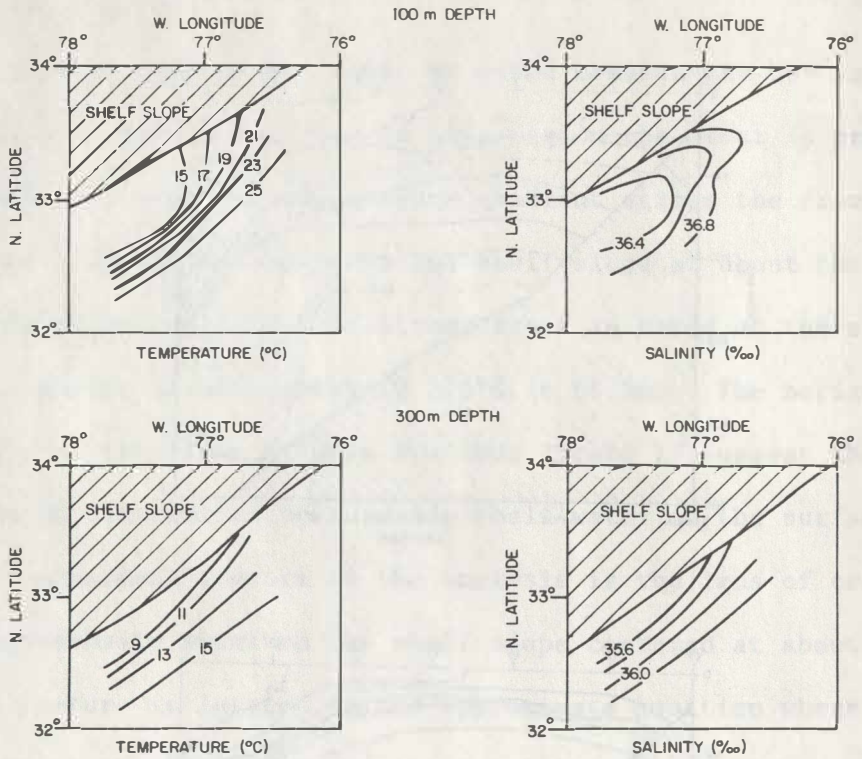

Figure 13. Temperature (oC) and salinity (‰) analysis at the 100-m and 300-m depth using data from Transects 1 and 2.

about the same as that in the satellite data if symmetry is assumed. A dome of cold, low-salinity water is a feature also associated with cyclonic cold eddies found on the eastern side of the Gulf Stream (Vukovich, 1976, and Vukovich and Crissman, 1978). This characteristic provides a strong indication of cyclonic motion. Cyclonic motion in western boundary eddies was suggested by Stumpf and Rao (1975), Legeckis (1979), and others.

There was no suggestion of a tongue of high-salinity water extending shoreward from the high-salinity core of the Gulf Stream in the analysis of the data from Transect 2. If there is cyclonic motion in the eddy, the data in Figure 15 suggest that Transect 1 would be in a region of shoreward motion associated with that circulation whereas Transect 2 would be in a region where the motion was generally parallel to the direction of motion of the Gulf Stream. This would account for the presence of the tongue of high-salinity water in the analysis along Transect 1 and the absence of it in the analysis along Transect 2.

Figure 14 shows the analysis of the data collected along Transect 3. Data were collected at 9 stations about 15 km apart. This transect is very near Transect 2, but the data were collected 7 days later. The data-collection period was 2006 EST on 19 May 1977 to 1524 EST on 20 May 1977. As indicated, the western boundary eddy remained stationary over the period, and the comparison between the analysis along Transects 2 and 3 will provide information on the time variation of the physical structure in a region near the center of the eddy.

In these analyses, there is no indication of the warm, high-salinity, low-density water on the shelf. Possibly the transect did not extend far enough shoreward. The intense subsurface front indicated in the analysis of

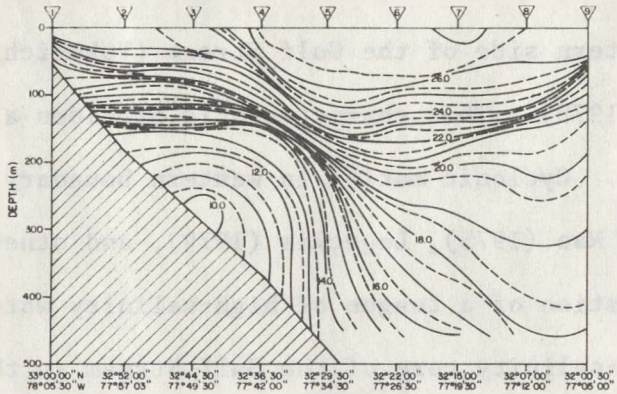

(A)

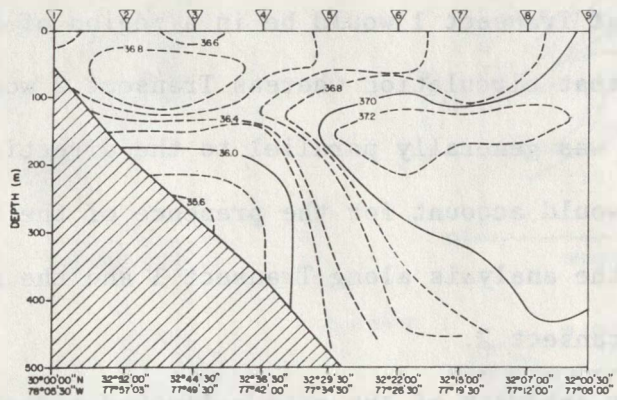

(B)

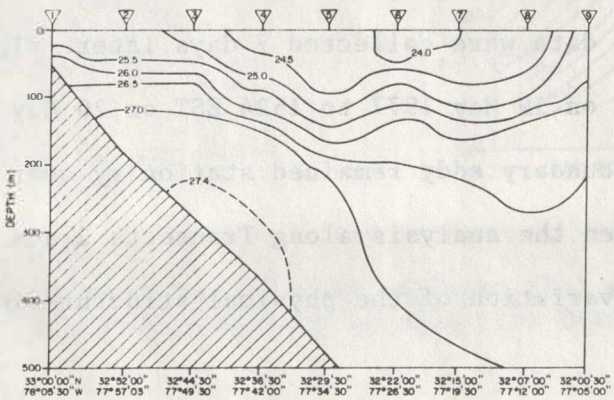

(C)

Figure 14. Cross-sectional analysis of (A) temperature (^{o}C), (B) salinity (‰), and (C) density (σ_t) along Transect 3

the data along Transect 2 had apparently weakened. The vertical temperature change shoreward from Station 4 is not as strong in the region between the 50- and 75-m depth (approximately 3°C) as it was along Transect 2. However, the isotherms are still parallel to the depth contours in that region.

The subsurface lens, and accompanying dome, of cold, low-salinity, high-density water on the shelf slope is still present, but the lens is smaller. Over the 7-day period, the temperature in the center of the lens had increased by approximately 1°C and the salinity had increased by approximately 0.1 parts per thousand. Differences are most likely due to diffusion of heat and mass. The center of the lens is located at approximately the 275-m depth along Transect 3 and was located at approximately a 325-m depth along Transect 2. This would suggest that the lens rose vertically over the 7-day period at an average speed of approximately 0.1 mm s^{-1} (about 1 m day^{-1}).

The other interesting feature noted in the analysis, which was not present in the analysis of the data from Transect 2, was the subsurface lens of high-salinity water located at Stations 2 and 3. The only apparent source of this high salinity is the high-salinity core of the Gulf Stream. However, it may be a result of an overriding of low-salinity water from the shelf.

5.2.3 Circulation Features

In order to obtain information on the surface circulation associated with the western boundary eddy, two satellite-tracked, free-drifting buoys (the drogue was set at the 3-m depth) were launched in the eddy, one along each transect. Figure 15 is the 11 May sea surface temperature analysis from NOAA-5 infrared data with the buoy track superimposed. It should be noted that the buoy track covers a period of at most 7 days. During the

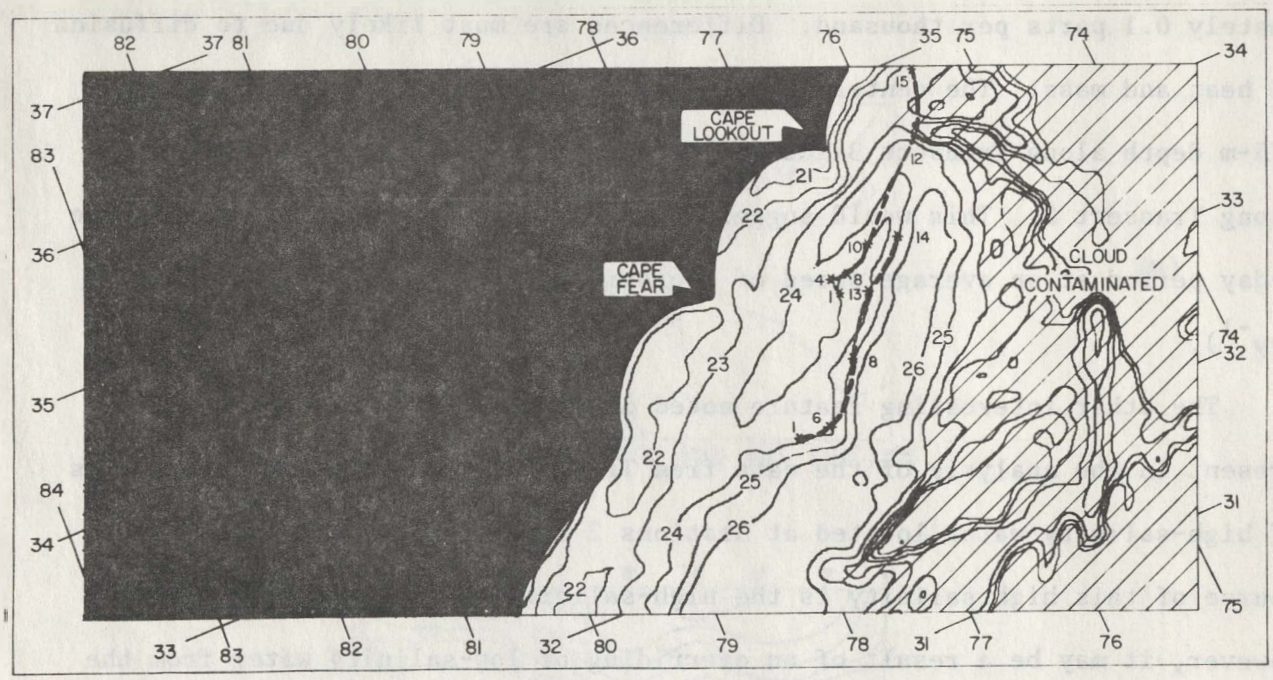

Figure 15. NOAA-5 sea-surface temperature (^{o}C) analysis for 11 May 1977 with free-drifting buoy tracks superimposed.

7-day period, marked changes in the sea-surface temperature structure as depicted in the 11 May analysis may have occurred in the regions to the north of the wave crest.

The first buoy was launched on 12 May at 0815 EST along Transect 1. The initial launch position was approximately 33.6°N and 76.9°W. Table 3 yields data on the position of the buoy versus time. Because of the scale of the map used for Figure 15, not all positions could be plotted. Those not plotted did not add anything crucial to the analysis. For the first 4 days, the buoy drifted slowly (the average speed was on the order of 16 cm s^{-1}) east-northeast. During this period, the southeast coast was influenced by a cold frontal passage. The high winds from the north may have influenced the motion of the buoy. On 16 May, the buoy accelerated in the northeast direction, having an average speed of approximately 200 cm s^{-1} over the next 24 hours. During this period, the data indicate that the buoy, which was in the cold tongue, penetrated across the warm tongue as shown in the 11 May analysis. On 16 and 17 May, the winds were generally out of the north and were weak, ruling out the possibility that the buoy was blown across isotherms. There was probably a change in the surface thermal structure and the cold tongue merged with the shelf water, which would explain the buoy's behavior. Such effects have been noted before (Vukovich and Crissman, 1975). After 17 May, the buoy slowed down and moved in an east-northeast direction with an average speed of approximately 65 cm s^{-1} over the next 24 hours. After 18 May, no usable data were received. It should be noted that prior to the period the buoy began to move across isotherms, the buoy trajectory was parallel to the isotherm configuration in the 11 May analysis.

TABLE 3. POSITIONS OF THE BUOY LAUNCHED ALONG TRANSECT 1 VERSUS TIME*

Location Number	Date (Mo/Day)	Time (EST)	Latitude (°N)	Longitude (°N)
†1	5/12	0815	33.61	76.91
2	5/12	0853	33.59	76.93
3	5/12	2342	33.63	76.90
4	5/13	0813	33.67	76.86
5	5/13	0955	33.67	76.85
6	5/13	2302	33.72	76.86
7	5/14	0915	33.72	76.79
8	5/14	2220	33.73	76.74
9	5/15	0834	33.75	76.63
10	5/15	1020	33.76	76.46
11	5/15	1206	33.76	76.50
12	5/16	0754	34.35	75.79
13	5/16	0936	34.43	75.76
14	5/16	2057	34.85	75.53
15	5/16	2243	34.85	75.52
16	5/17	0857	34.93	75.48
18	5/17	2201	35.10	75.29
19	5/18	0916	35.21	75.15

*Some erroneous positions have been removed from the data set.

†Launch position.

The second buoy was launched on 13 May at 0700 EST along Transect 2. The initial launch position was approximately 32.7°N and 77.7°W. Table 4 gives information on the buoy position versus time. In the first 24 hours, the buoy moved eastward, a direction consistent with the orientation of the surface isotherms in that region. The average speed of the buoy was approximately 34 cm s^{-1}. After 14 May, the buoy moved northeastward, a direction also consistent with the orientation of the isotherms in this region. The buoy was still moving northeastward on 18 May, the last day usable position data were received. During that period the average speed of the buoy was approximately 60 cm s^{-1}.

Geostrophic currents were computed relative to the 500-m depth or the local bottom, whichever came first. Positive motion is eastward and negative motion, westward. In this region, the geostrophic current is governed by the Gulf Stream, which generally flows from the southwest to the northeast. However, since Transects 1 and 2 are oriented north-south and the geostrophic motion is relative to the transect, only eastward or westward components of the motion can be accounted for.

Figure 16 shows the horizontal analysis of the surface geostrophic speed obtained using the transect computations. Two important features are noted in this analysis. The first is a region of negative geostrophic speed centered about the shelf break (200-m isobath). The maximum speed in this region is on the order of 10 cm s^{-1}. The location of the negative motion correlates well with the position of the warm tongue found in 11 May sea-surface temperature analysis (Figure 12). The other feature is the large positive geostrophic speed found in the Gulf Stream near the crest of the wave associated with the perturbation. The maximum speed in this region is on the order of 160 cm s^{-1}.

TABLE 4. POSITIONS OF THE BUOY LAUNCHED ALONG TRANSECT 2 VERSUS TIME*

Location Number	Date (Mo/Day)	Time (EST)	Latitude (°N)	Longitude (°N)
†1	5/13	0700	32.73	77.68
3	5/13	0959	32.71	77.73
4	5/13	2302	32.65	77.64
5	5/14	0051	32.64	77.57
6	5/14	0914	32.73	77.39
7	5/14	2222	32.95	77.09
8	5/15	0837	33.09	77.03
9	5/15	1019	33.13	76.81
10	5/15	1205	33.11	76.96
12	5/16	0938	33.23	76.92
13	5/17	0859	33.49	76.62
14	5/17	2351	33.83	76.23

*Some erroneous positions have been removed from the data set.

†Launch position.

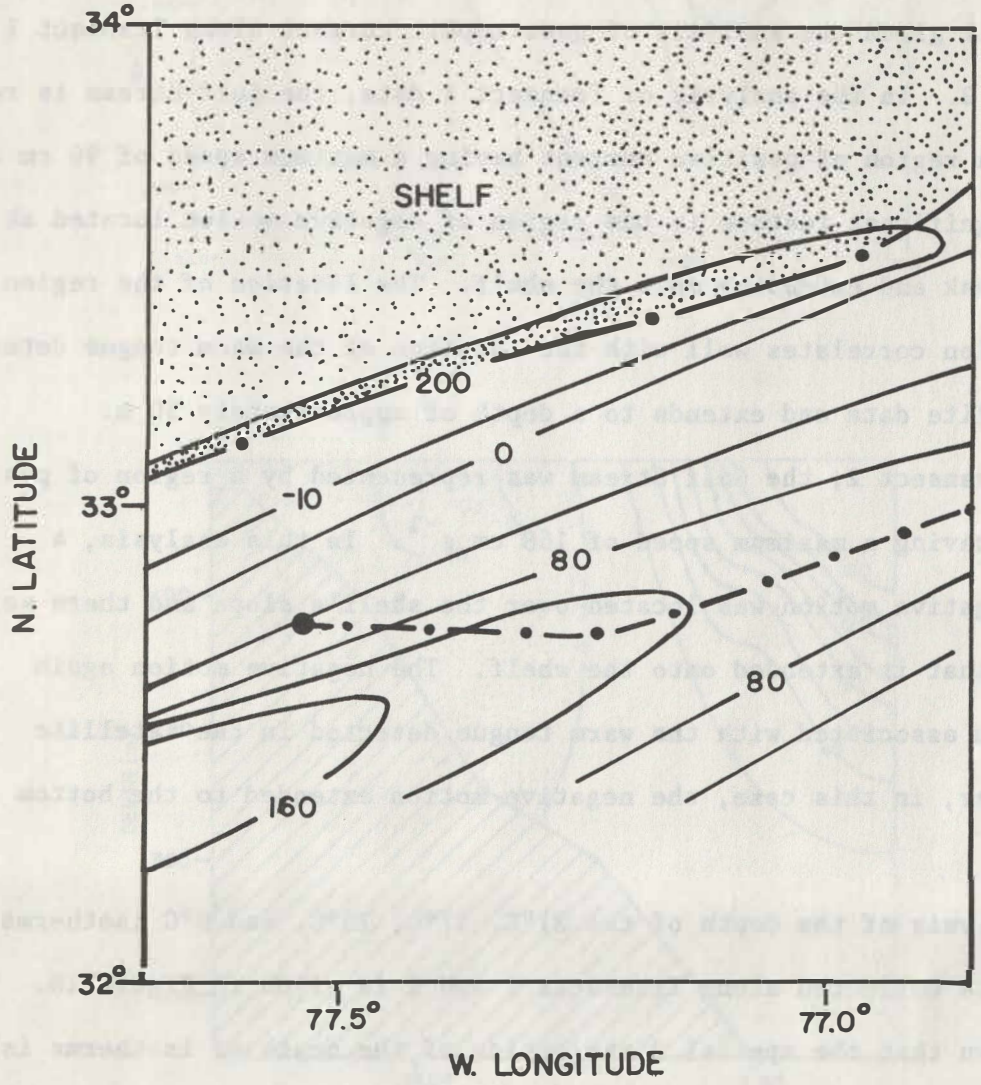

Figure 16. Analysis of geostrophic current (cm s^{-1}) at the surface using data from Transects 1 and 2. The dash-dot line is the path of the bouy launched along Transect 2. The large dot indicates the launch point.

Also shown in the figure is the trajectory of the buoy that was released along Transect 2. The mean speed of the buoy west of 77.4°W was 68 cm s^{-1} and the mean geostrophic current speed along the path of the buoy was about 60 cm s^{-1}. East of 77.4°W, the buoy had an average speed of 89 cm s^{-1}, and the mean geostrophic current along the path was about 90 cm s^{-1}. All in all the buoy and geostrophic speeds compared well.

Figure 17 gives the analysis of geostrophic current along Transect 1 and Transect 2. In the analysis of Transect 1 data, the Gulf Stream is represented by a region of positive current having a maximum speed of 90 cm s^{-1}. The other significant feature is the region of negative motion located at the shelf break and extending onto the shelf. The location of the region of negative motion correlates well with the location of the warm tongue detected in the satellite data and extends to a depth of approximately 50 m.

Along Transect 2, the Gulf Stream was represented by a region of positive motion having a maximum speed of 168 cm s^{-1}. In this analysis, a region of negative motion was located over the shelf's slope and there were indications that it extended onto the shelf. The negative motion again appears to be associated with the warm tongue detected in the satellite data. However, in this case, the negative motion extended to the bottom (175 m).

The analysis of the depth of the 21°C, 17°C, 13°C, and 9°C isotherms using the data collected along Transects 1 and 2 is given in Figure 18. It has been shown that the spatial distribution of the depth of isotherms is to some extent correlated with the spatial distribution of the dynamic topography or the streamlines of flow. The depth analysis of all four isotherms

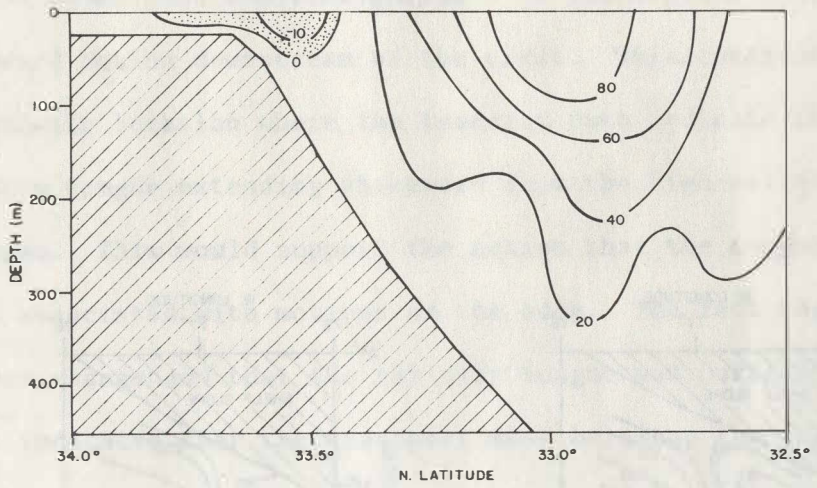

(A)

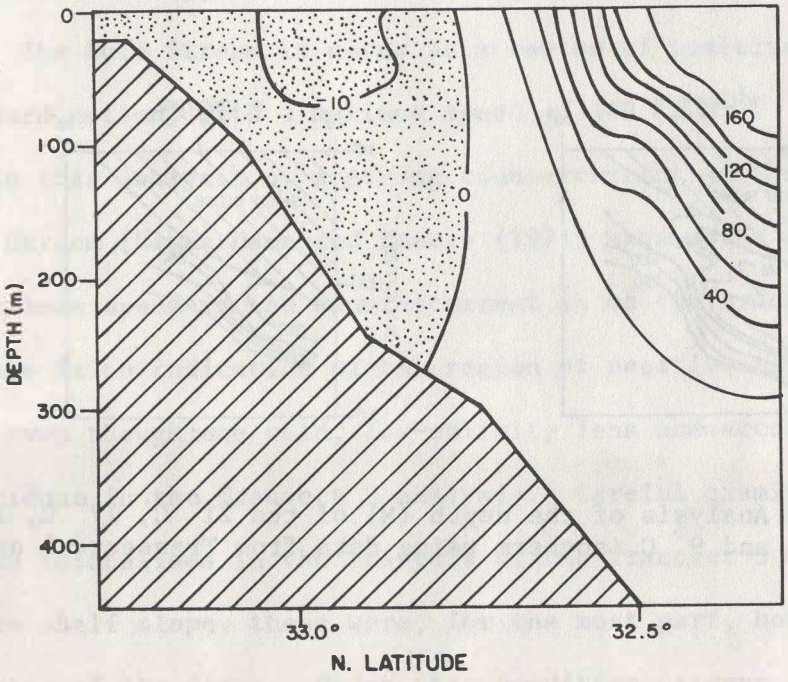

(B)

Figure 17. Analysis of geostrophic current (cm s^{-1}) along Transects 1 (A) and 2 (B)

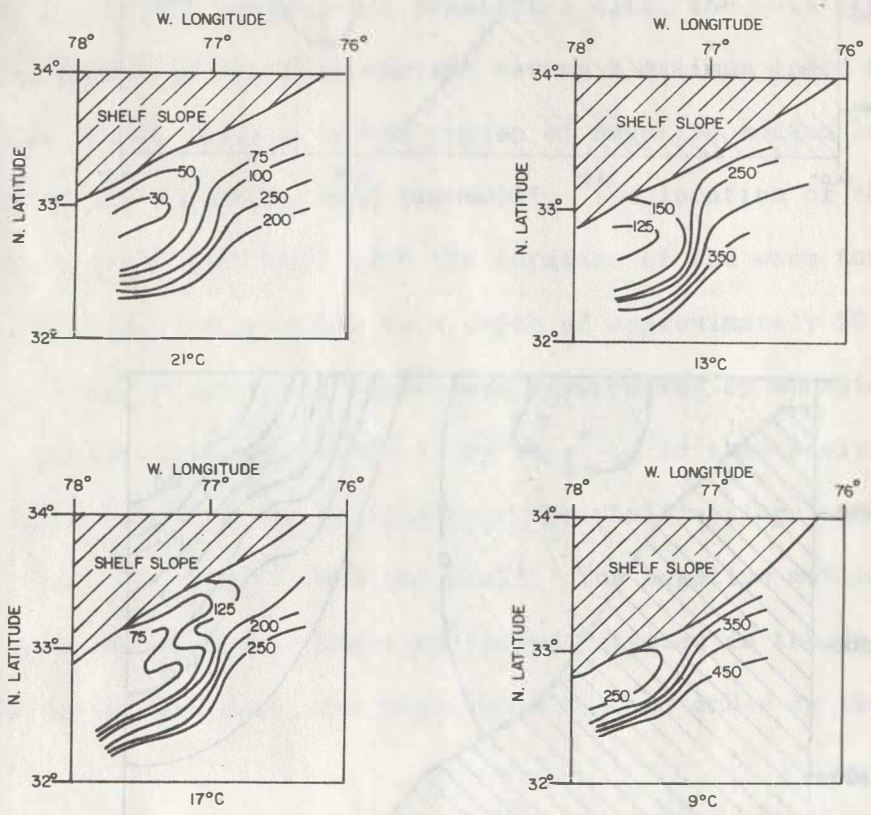

Figure 18. Analysis of the depth (M) of the 21° C, 17° C, 13° C, and 9° C isotherm using data from Transects 1 and 2

show a region of small values of isotherm depth centered where the wave was detected in the satellite data. This feature is characteristic of cyclonic motion. It is noted that the configuration of the depth contour suggests strong shoreward motion downstream of the crest. This configuration exists in the approximate location where the transect data indicate the presence of a high-salinity tongue extending shoreward from the high-salinity core of the Gulf Stream. This would support the notion that the tongue may be due to transport associated with motions in the eddy. The fact that there was no temperature change and that the salinity tongue was parallel to the Gulf Stream front indicates that the transport must be along the front.

The analysis of the geostrophic currents along Transect 3 is given in Figure 19. As indicated earlier, these data were collected 7 days after the data were collected along Transect 2 and in the approximate location as Transect 2. The Gulf Stream is noted as a region of positive motion (approximately eastward motion) with a maximum speed of 149 cm s^{-1}. There is an indication in this analysis of a strong countercurrent on the eastern side of the Gulf Stream [Richardson and Knauss (1971) have noted this feature before]. Maximum speed in the countercurrent is on the order of 100 cm s^{-1}. However, there is no indication of the region of negative motion over the shelf slope even though the cold, low-salinity lens and accompanying dome was still evident in the Transect 3 analysis. Careful examination of the isotherms and iosohalines in the analysis of the Transect 3 data indicate that over the shelf slope, these were, for the most part, horizontal except near the center of the domes. Under this condition, strong countermotions over the shelf slope are not expected.

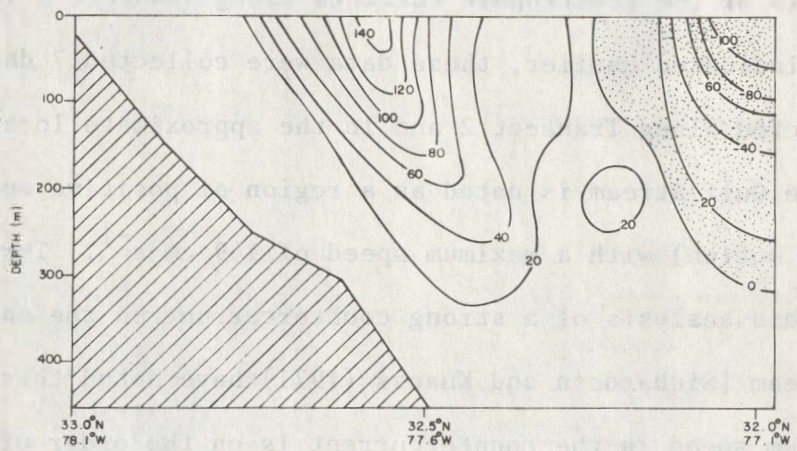

Figure 19. Analysis of geostrophic current (cm s^{-1}) along Transect 3

5.3 The 14 April 1977 Case Study

On 12 April 1977, an eddy was detected on the western boundary of the Gulf Stream using satellite data (Figures 7 and 8). The position of the eddy was approximately east of Onslow Bay about 330 km downstream of the Charleston Bump. The field program was initiated immediately to collect *in situ* data. Four transects were accomplished in the region of interest. Transect 1 was located upstream of the eddy because the eddy had moved north and eastward of its 12 April position according to the 14 April image (Figure 9). The position on the 14 April was approximately east of Cape Lookout, North Carolina. The three remaining transects were through the heart of the eddy.

5.3.1 Satellite Sea-Surface Temperature Analysis

The sea-surface temperature analysis obtained using digitized NOAA-5 infrared data for 14 April is given in Figure 20. Clouds obscured the northern and southern portions, but the region along the coast was clear. The Gulf Stream is represented as a long tongue of warm water having a temperature on the order of 26°C. Cold water characterized the coastal regions with temperatures on the order of 20°C. The particular western boundary eddy of interest was located east of Cape Lookout, centered at approximately 34.25°N and 76°W. The eddy appeared simply as a waveform with no associated cold and warm tongues as in the 11 May case study. The wavelength was approximately 160 km. It is noted that a cold lens is located in the eddy immediately downstream of the crest. The temperature in the lens is less than 23°C. The lens was first detected in the 10 April infrared data (Figure 4) and persisted through 15 April (a minimum of 5 days), which was when the last clear sky image was available for the eddy of interest. After 15 April, clouds obscured the coastal regions for about 14 days. It

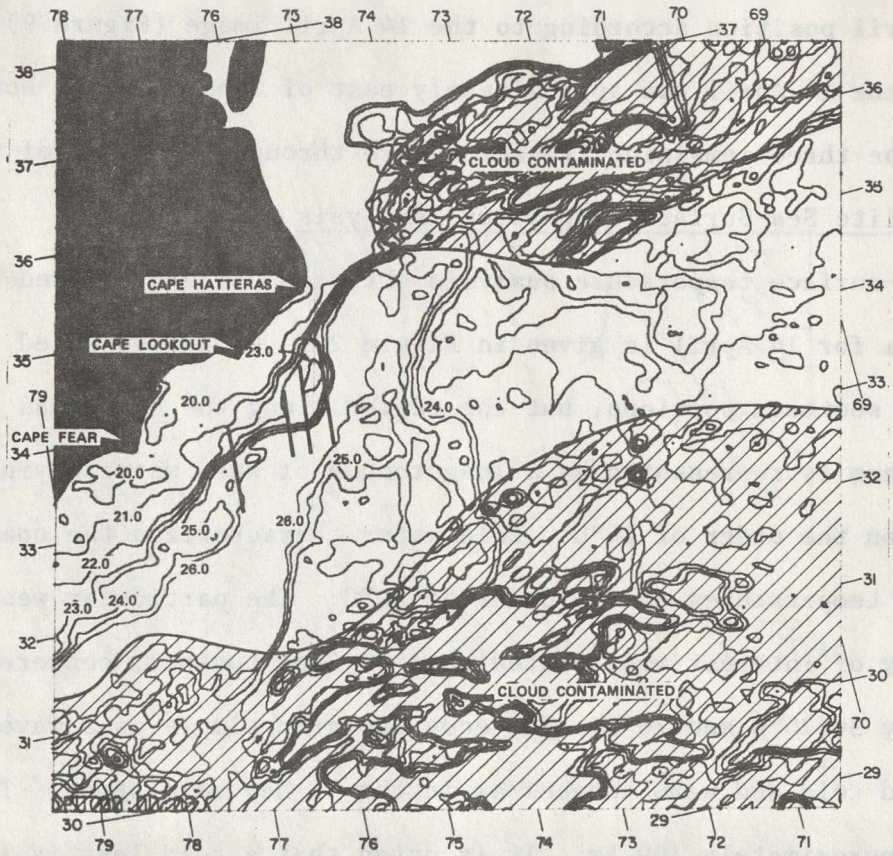

Figure 20. NOAA-5 sea-surface temperature (^{o}C) analysis for 14 April 1977

should be noted that there are two other western boundary eddies indicated in the data. Both of these are located upstream from the eddy of principal interest.

The solid lines in the figure denote the position of the four transects. Transect 1 is along the 76.75°W longitude line, east of that is Transect 2 along the 76.0°W longitude, east of that is Transect 3 along the 75.75°W longitude, and east of that is Transect 4 along the 75.5°W longitude. As indicated earlier, Transect 1 was performed upstream from the eddy of interest but also downstream from another eddy. There are indications in the satellite data of the existance or the development of a warm tongue in that region.

5.3.2 Subsurface Structure

The temperature, salinity, and density distribution along Transect 1 is shown in Figure 21. Data were collected at eight stations approximately 14 km apart along the 76.75°W longitude line from 33°N to 34°N. The transect was accomplished during the period 1955 EST on 14 April to 1000 EST on 15 April.

The data give no indication of warm, high-salinity, low-density water on the shelf as previously noted in the 11 May case study of western boundary eddies. This factor was also indicated in the satellite data (Figure 20). It is noted that there is a strong thermal front at the surface between Stations 2 and 2a. The temperature gradient across the front is approximately 6°C in 8 km. Apparently, this is the surface manifestation of the Gulf Stream front. The data also indicate that there exist a low-salinity, low-density lens in the region around Stations 2 and 3. The lens is located in an area where the satellite data (Figure 20) indicate that there may be reminants of a warm tongue or that a warm tongue was developing. There are

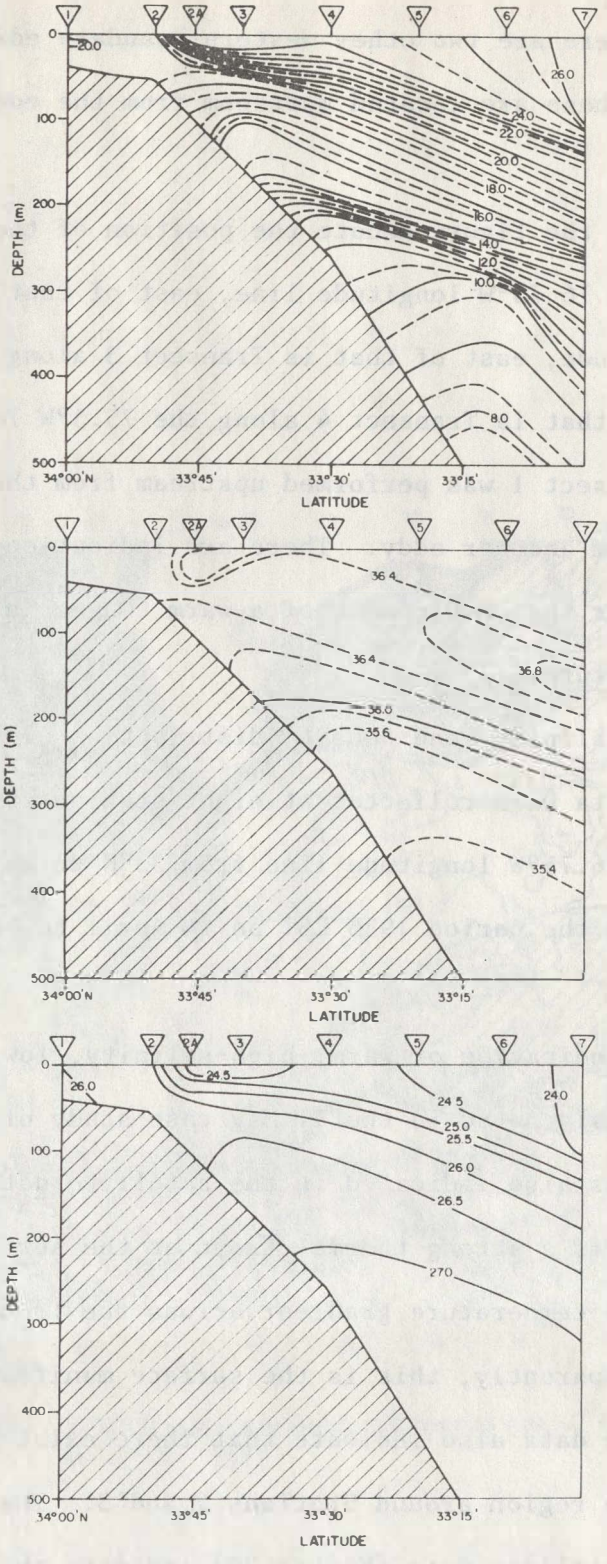

Figure 21. Cross-sectional analysis of (A) temperature (^{o}C), (B) salinity (‰), and (C) density (σ_t) along Transect 1

also indications in the surface layer of cold, high-density, high-salinity water separating the lens of low-salinity, low-density water from the Gulf Stream water.

A weak dome of cold, low-salinity, and high-density water appears to be located on the shelf's slope at Station 3 at around 150-m depth. There is also some indication of a dome of cold water at Station 6 below the 300-m depth. The salinity/density data have only weak indications of that dome.

There are indications of a high-salinity tongue extending shoreward from the high-salinity core of the Gulf Stream. The high-salinity core of the Gulf Stream is centered at around 150-m depth at Station 7. The analysis would indicate that the tongue extends from the high-salinity core of the Gulf Stream onto the shelf, being interrupted only by the lens of low-salinity, low-density water located around Stations 2 and 3.

The analysis of data along Transect 2 is presented in Figure 22. Four stations were accomplished approximately 27 km apart and along the 76°W longitude line from 33.5°N to 34.25°N. Data were collected in the period 0330 EST to 1030 EST on 17 April. The transect is in the upstream portion of the eddy. The eddy is located in a region where the slope is steep because the bottom topography is no longer influenced by the Blake Plateau.

There is no indication of warm, high-salinity, low-density water near the shelf. The surface manifestation of the Gulf Stream front is located between Stations 25 and 26. The gradient is on the order of 4°C in 27 km. There is also no indication of the cold, low-salinity, high-density lens or dome on the shelf's slope. Seaward from the slope, a broad region of cold, low-salinity, and high-density water separates the Gulf Stream from the slope. In this region, the isotherms, isohalines, and isopycnals are almost

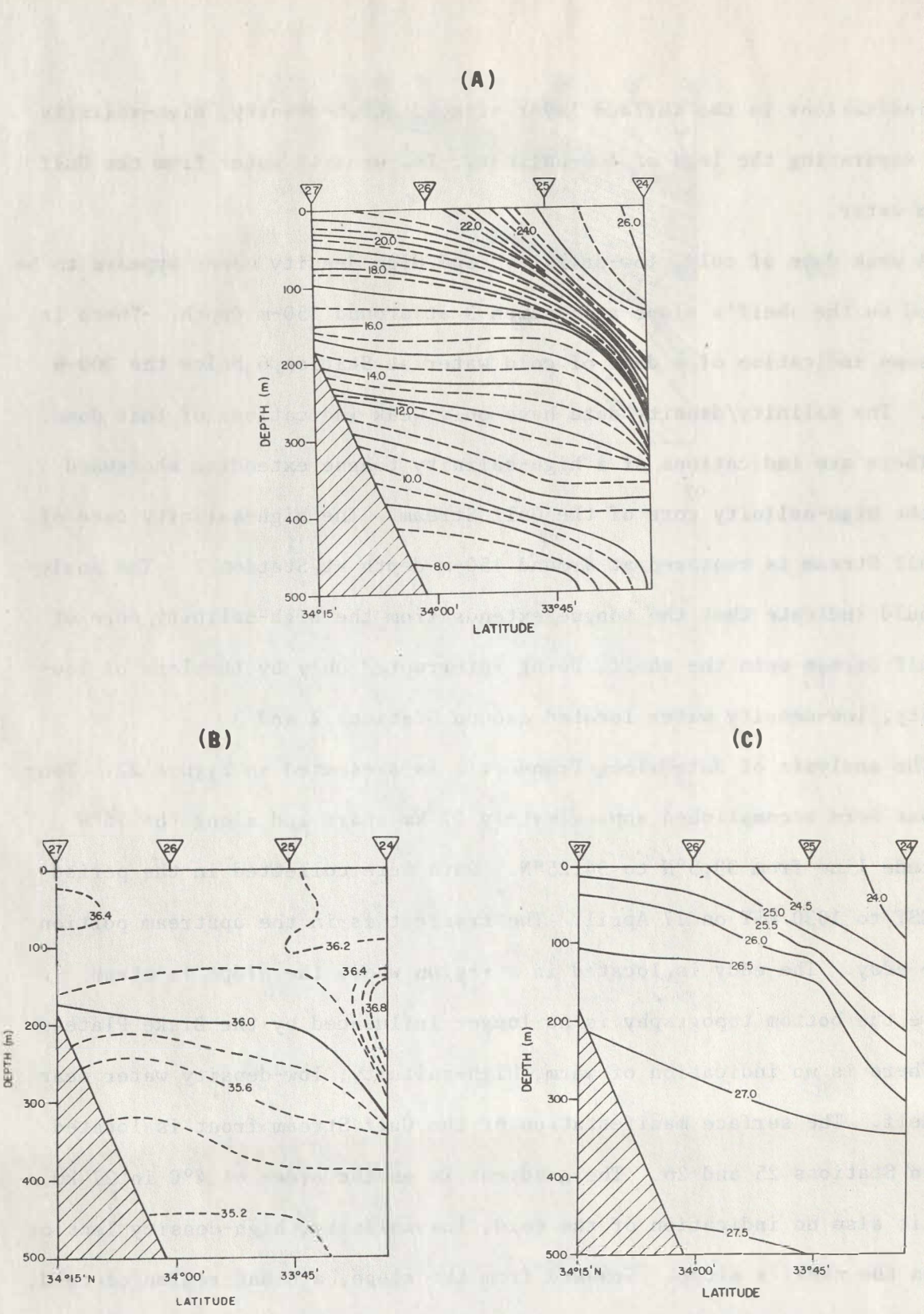

Figure 22. Cross-sectional analysis of (A) temperature (^{o}C), (B) salinity (‰), and (C) density (σ_t) along Transect 2

horizontal. Based on these data alone, it is difficult to establish an association between this feature and the wave at the surface.

There are indications of a high-salinity tongue extending shoreward from the high-salinity core of the Gulf Stream. Associated with this tongue is a broad region of high salinity extending shoreward from Station 25 and extending from the surface to the 150-m depth. There is also a high-salinity lens in the subsurface centered at around the 50-m depth at Station 27. The data were not sufficient to determine the relationship between the salinity in the high salinity core and that in the surface layer north of Station 25.

The analysis of the data collected along Transect 3 is given in Figure 23. Data were obtained at seven stations approximately 20 km apart along the 75.75°W longitude line from 33.5°N to 34.75°N. Data were collected in the period 1422 EST on 16 April to 0205 EST on 17 April. The transect was initiated in a region immediately upstream from the crest of the wave and proceeded to the heart of the eddy.

There are indications of warm, high-salinity water shoreward of Station 18 in the surface layer. This water mass is relatively shallow. Thermal structure suggests that it is 20 m deep and the salinity structure, 30 m deep. The surface manifestation of the Gulf Stream front is located between Stations 18 and 19 and has a gradient of approximately 3°C in 20 km. The satellite data indicate that the cold water separating the warm water shoreward from Station 18 and the Gulf Stream front, is that water found in the cold lens located immediately downstream from the center of the eddy. The analysis indicates the presence of strong subsurface fronts associated with the Gulf Stream between Stations 19 and 20.

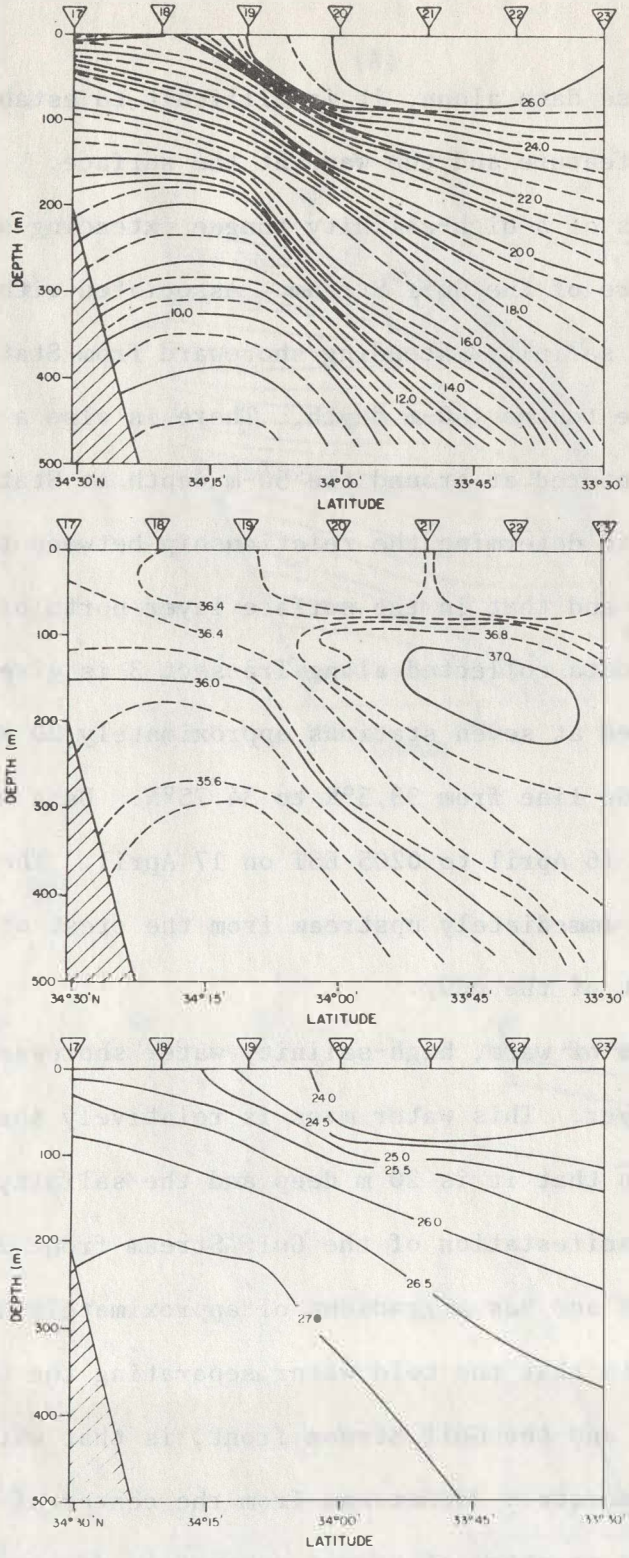

Figure 23. Cross-sectional analysis of (A) temperature (^{o}C), (B) salinity (‰), and (C) density (σ_t) along Transect 3

There is a dome of cold, low-salinity, high-density water located seaward from the slope. The dome is centered at around Station 18, and is most pronounced below the 200-m depth. This structure is significantly different than that found in the 11 May case, in that the lens and accompanying dome of cold, low-salinity, high-density water was centered on the shelf's slope at around the 325-m depth in that case. The dome associated with this western boundary eddy extends to greater depths.

There also appears to be a tongue of high-salinity water extending shoreward from the high-salinity core of the Gulf Stream. The tongue apparently reaches the surface at around Stations 17 and 18. However, the data were not sufficient to confirm or deny that the salinity in the surface layer at Stations 17 and 18 originate from the high salinity core of the Gulf Stream.

The analysis of the data along Transect 4 is given in Figure 24. This transect was accomplished along the 75.5°W longitude line from 33.5°N to 34.75°N. There were nine stations along the transect approximately 15 km apart, and the data were collected in the period 1712 EST on 15 April to 0900 EST on 16 April. This transect essentially passes through the downstream portion of the western boundary eddy.

There is a region between Stations 14 and 16 characterized by alternating cold, high-density and warm, low-density water in the near surface layer. The salinity at the surface at Stations 14 and 15 is the largest surface value experienced along this transect. Note that the surface salinity in the broad region between Stations 13 and 16 is high relative to the surface values in the Gulf Stream. Though this feature appears somewhat similar to the alternating cold and warm water feature found in the 11 May

(A)

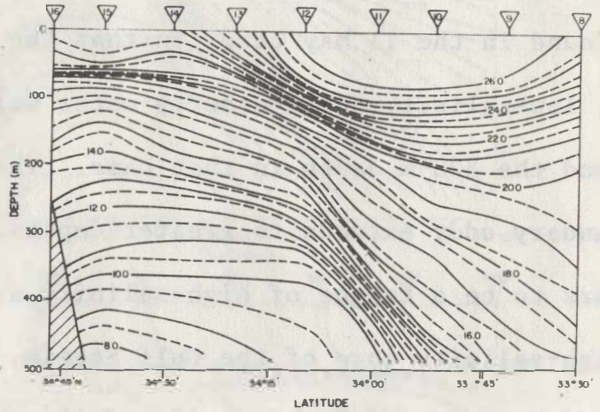

(B)

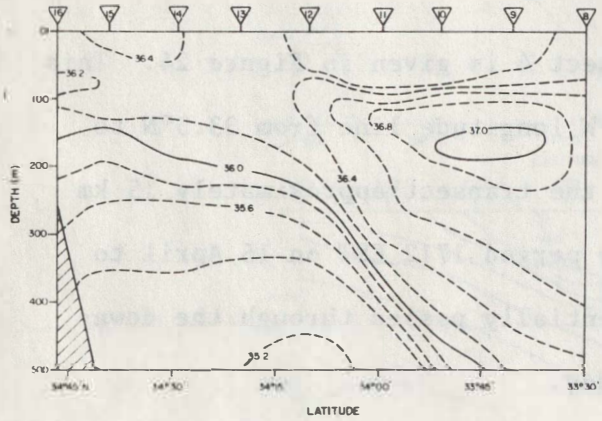

(C)

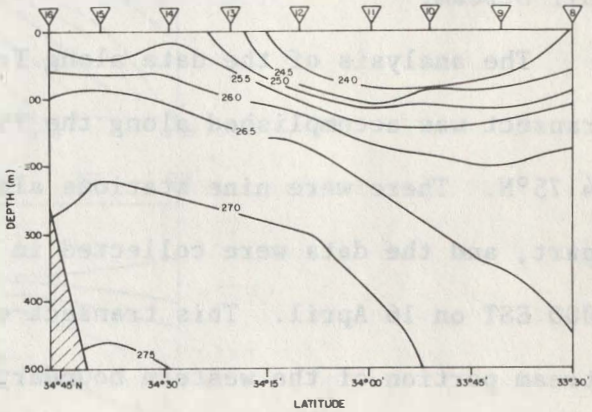

Figure 24. Cross-sectional analysis of (A) temperature (^{o}C), (B) salinity (‰), and (C) density (σ_t) along Transect 4

case, neither the satellite data nor the in situ data indicate that this is that type of feature.

The surface manifestation of the Gulf Stream front is found between Stations 12 and 14. The thermal gradient is on the order of 6°C in approximately 30 km. There are strong subsurface fronts located at Station 12 at the 75-m depth, and at Station 11 at the 350-m depth.

A dome of cold, low-salinity, high-density water is found below the 100-m depth and between the slope and the Gulf Stream. The thermal dome is centered near the slope at Station 15. However, the center of low salinity is displaced further offshore of the slope at Station 12.

There are also indications of a tongue of high-salinity water in the subsurface extending from the high-salinity core of the Gulf Stream shoreward and upward to the surface. The analysis would suggests that this tongue would account for the high salinity found at Stations 14 and 15. However, there were no data available to support this contention.

Figure 25 yields the horizontal analysis of temperature and salinity at the 100- and 300-m depths. The data for these analysis were obtained from the four transects. This analysis supports the cross-sectional analyses in that the cold, low-salinity dome was most evident below the 100-m depth.

5.3.3 Circulation Features

A satellite-tracked free-drifting buoy was launched on 14 April at 2224 EST along Transect 1 in order to study the circulation associated with the western boundary eddy. Figure 26 is the 14 April sea-surface temperature analysis with the buoy track superimposed. The buoy was launched on the shoreward side of the Gulf Stream's western boundary at approximately 33.76°N and 76.76°W. The buoy track covers a 14-day period; after 28 April,

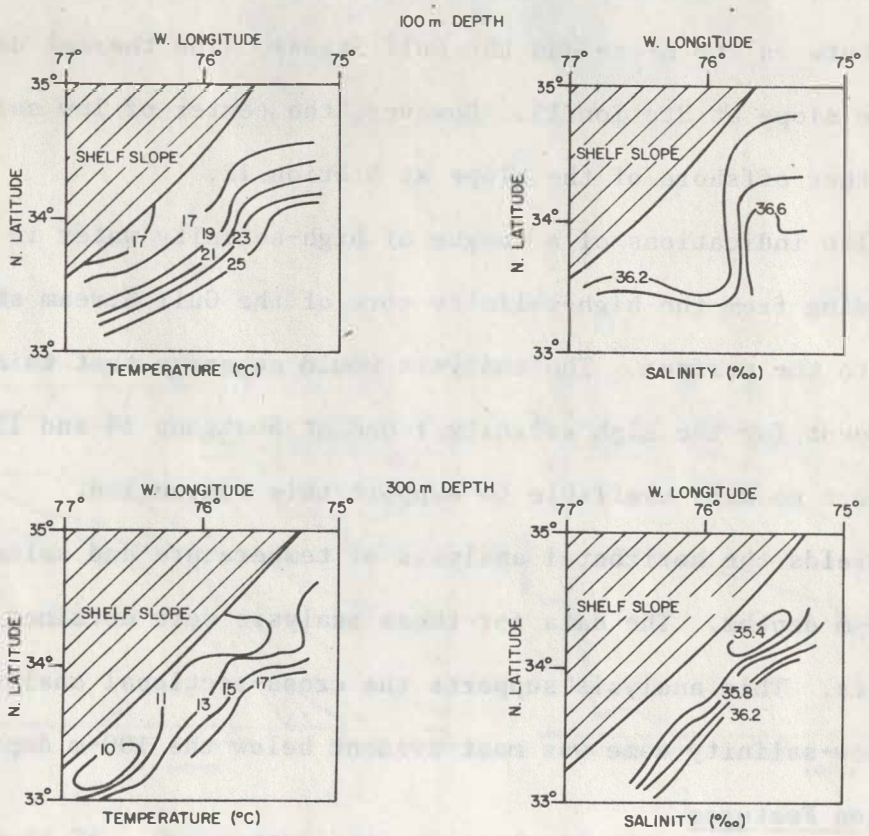

Figure 25. Temperature (^{o}C) and salinity (‰) analysis at the 100-m and 300-m depth using data from Transects 1 through 4

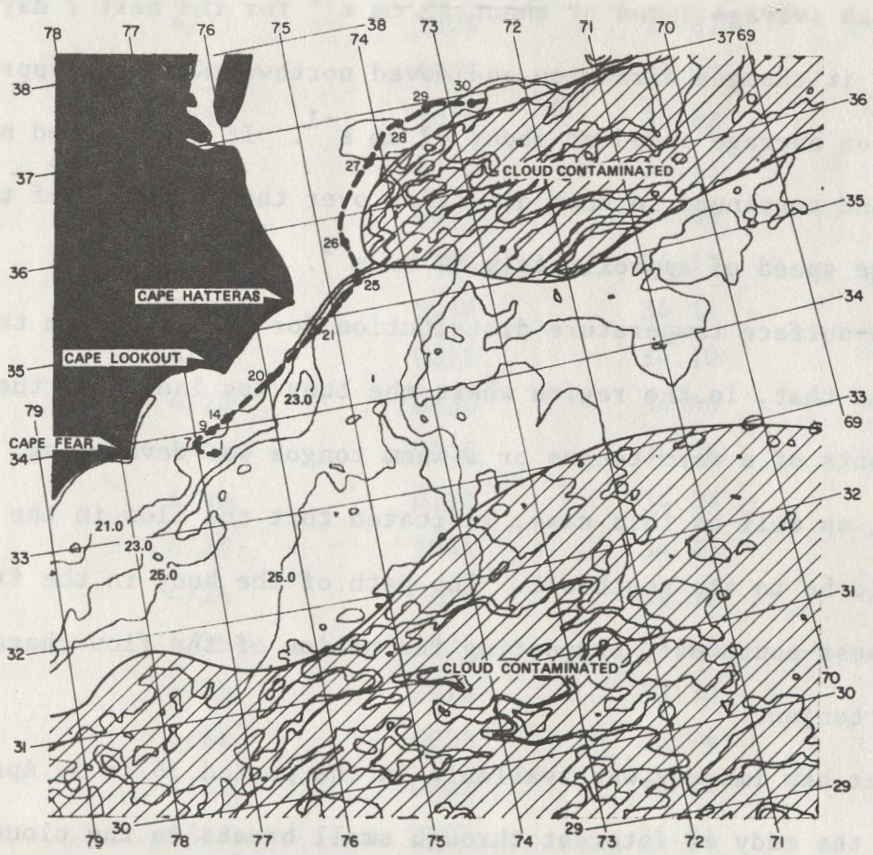

Figure 26. NOAA-5 sea-surface temperature (°C) analysis for 14 April 1977 with free-drifting buoy track superimposed

there was an apparent instrument failure on the buoy because transmission ceased. Table 5 yields the position versus time of the buoy over the 14-day period.

Examination of the data in Table 5 will show that initially the buoy moved west-southwestward, at approximately 16 cm s^{-1} for the first 3 days (this is not evident in Figure 28 because the scale of the map would not permit all positions to be plotted). After 18 April, the buoy moved northeastward at an average speed of about 22 cm s^{-1} for the next 7 days. Then on 25 April, it changed direction and moved northwestward for approximately 11 hours at an average speed of about 47 cm s^{-1}. It then turned northeastward again and continued in that direction over the remainder of the period at an average speed of approximately 30 cm s^{-1}.

The sea-surface temperature distribution for 14 April from the NOAA-5 data indicate that, in the region where the buoy was launched, there were either remnants of a warm tongue or a warm tongue was developing. The 11 May case, as well as this case, indicated that the flow in the warm tongue should be to the southwest. The path of the buoy in the first 3 days was to the west-southwest, supporting the notion of the flow characteristics in the warm tongue.

No clear sky imagery was available in the period 16 to 30 April, but glimpses of the eddy of interest through small breaks in the cloud cover over that period suggested that the eddy was located at 34.25°N and 74.25°W at around 28 April. Furthermore, estimates based on the speed of the eddy obtained during the period of 14 through 16 April indicated that the eddy would be at about that position around 28 April, provided the speed remained steady. In that region, the buoy track changes from a northeasterly direc-

TABLE 5. POSITIONS OF THE BUOY LAUNCHED ALONG TRANSECT 1 VERSUS TIME*

Location Number	Date (Mo/Day)	Time (EST)	Latitude (°N)	Longitude (°N)
†1	4/14	2224	33.76	76.76
2	4/15	0954	33.88	76.71
3	4/16	1054	33.91	76.84
4	4/16	2214	33.87	76.96
6	4/17	1203	33.87	76.99
7	4/18	0936	33.92	77.04
8	4/19	1038	34.02	76.97
9	4/19	2343	34.13	76.80
10	4/20	0815	34.06	76.80
12	4/20	2302	34.11	76.82
13	4/21	0918	34.11	76.85
16	4/21	2222	34.10	76.80
17	4/22	0836	34.08	76.78
18	4/22	2326	34.08	76.61
19	4/23	0112	34.09	76.60
20	4/24	1044	34.41	75.90
21	4/25	0819	34.82	75.21
23	4/25	1004	34.86	75.12
25	4/25	2310	35.30	74.46
26	4/26	0923	35.74	74.73
27	4/27	0842	36.46	74.02
28	4/27	2327	36.81	73.60
29	4/28	0945	36.98	73.32
30	4/28	2250	36.94	72.65

*Some erroneous positions have been removed from the data set.

†Launch position.

tion to a northwesterly direction, leaving the general impression of a wave form. The available imagery indicated that the directional change from northeast to northwest occurred at the crest of the wave and the northwest motion was in the downstream portion of the eddy. It should be noted that in the period 25-26 April, the speed of the buoy increased as it traversed through the eddy. During that period, the speed of the buoy was as large as 73 cm s^{-1}.

Figure 27 shows the horizontal analysis of the surface geostrophic speed obtained using transect data. The analysis shows no indication of countermotion at the shelf break (200-m isobath). Actually, there is a small region of negative motion in the northernmost portions of the analysis which will be more evident in the cross-sectional analysis of geostrophic current. However, there is an indication of a region of maximum current speed in the vicinity of the eddy of interest. In reality, it appears the current maximum is located in the upstream region of that eddy. A secondary positive maximum (60 cm s^{-1}) appears to be located at around 33.5°N and 76.75°W at the shelf break.

The buoy was launched on the shelf where no geostrophic calculations were made. It did not enter the domain of the geostrophic calculations given in Figure 27 until 10 days after the mean time of the transect data used to make the geostrophic calculations. It is known that the eddy in question moved, suggesting that the geostrophic current field changed markedly during the period. Therefore, it was not possible to compare geostrophic currents with speeds of the free drafting buoy.

Figure 28 gives the analysis of geostrophic current along Transects 1 and 2. Along Transect 1, the Gulf Stream is noted to be a region of posi-

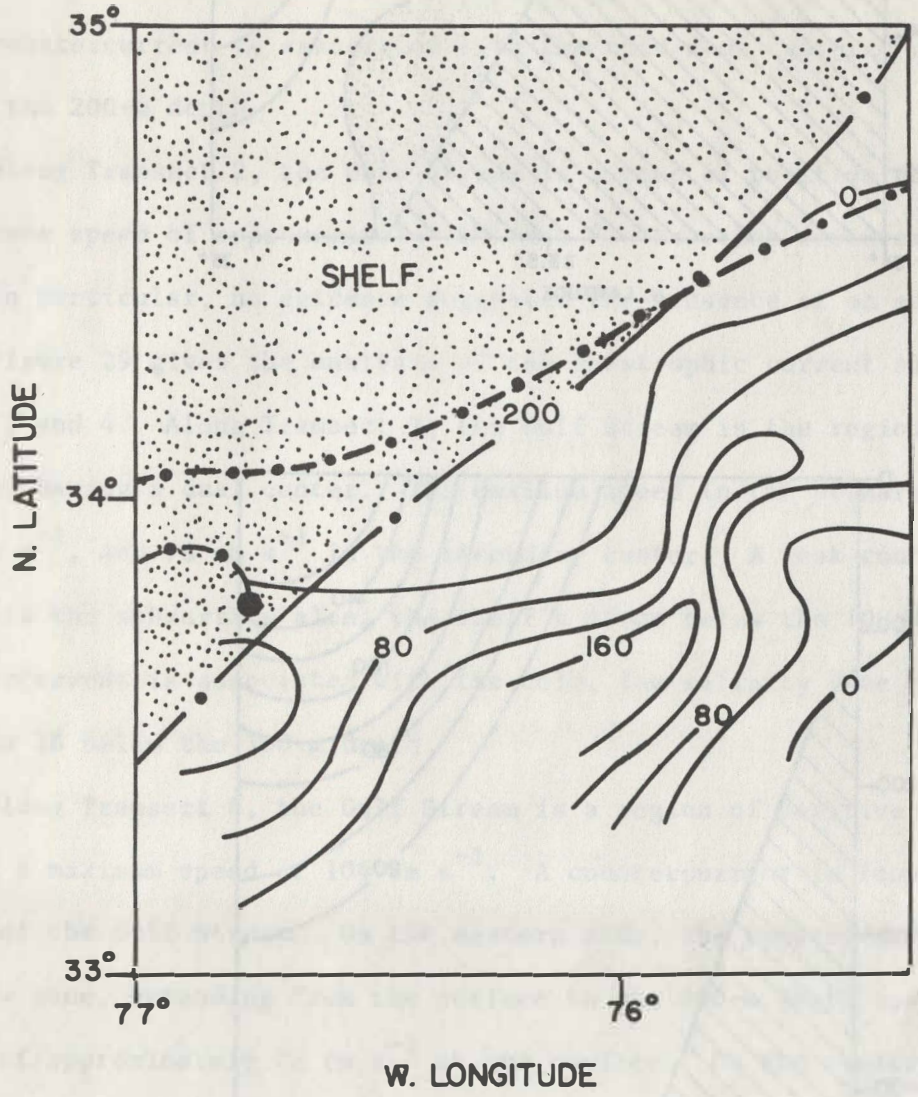

Figure 27. Analysis of geostrophic current (cm s^{-1}) at the surface using data from Transects 1 through 4. The dash-dot line is the path of the buoy launched along Transect 1. The large dot indicates the launch point.

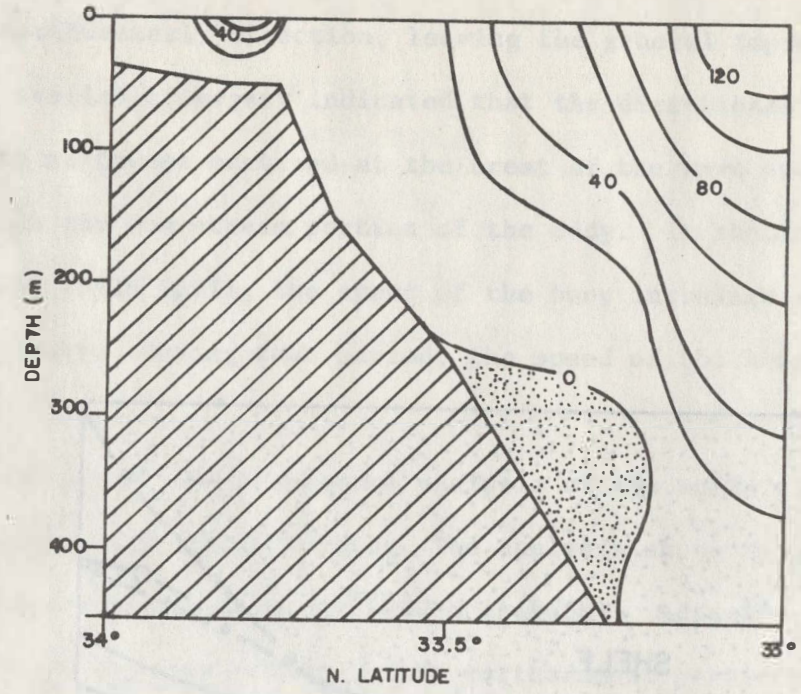

(A)

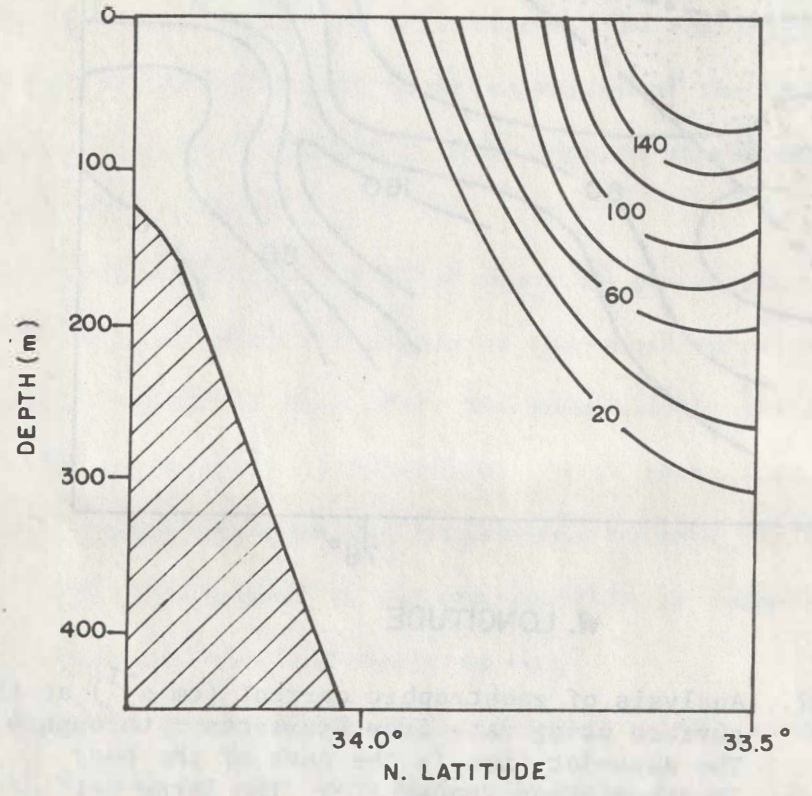

(B)

Figure 28. Analysis of geostrophic current (cm s^{-1}) along Transects 1 and 2

tive current having a maximum speed of approximately 132 cm s^{-1}. There is a secondary zone of strong positive current (maximum current speed of 60 cm s^{-1}) shoreward of the shelf break. This zone is shallow extending from the surface to approximately the 25-m depth. It is associated with the strong thermal front found at the surface in this region. A weak countercurrent is noted in the subsurface along the slope centered at about the 325 m depth. This countercurrent is associated with the cold dome centered at Station 6 below the 200-m depth.

Along Transect 2, the Gulf Stream is a zone of positive current having a maximum speed of approximately 169 cm s^{-1}. No other features were noted and, in particular, no evidence suggested the presence of an eddy.

Figure 29 gives the analysis of the geostrophic current along Transects 3 and 4. Along Transect 3, the Gulf Stream is the region of positive current having a dual center. The maximum speed in the primary center is 131 cm s^{-1}, and 78 cm s^{-1} in the secondary center. A weak countercurrent is noted in the subsurface along the shelf's slope below the 100-m depth. The countercurrent is associated with the cold, low-salinity dome centered at Station 18 below the 100-m depth.

Along Transect 4, the Gulf Stream is a region of positive current having a maximum speed of 104 cm s^{-1}. A countercurrent is found on both sides of the Gulf Stream. On the eastern side, the countercurrent is a shallow zone, extending from the surface to the 100-m depth having a maximum speed of approximately 22 cm s^{-1} at the surface. On the western side, a weak countercurrent is located over the shelf break from the surface to the 250-m depth. The maximum speed is found at the 75-m depth and is 10 cm s^{-1}. This countercurrent appears to be associated with the cold, low-salinity

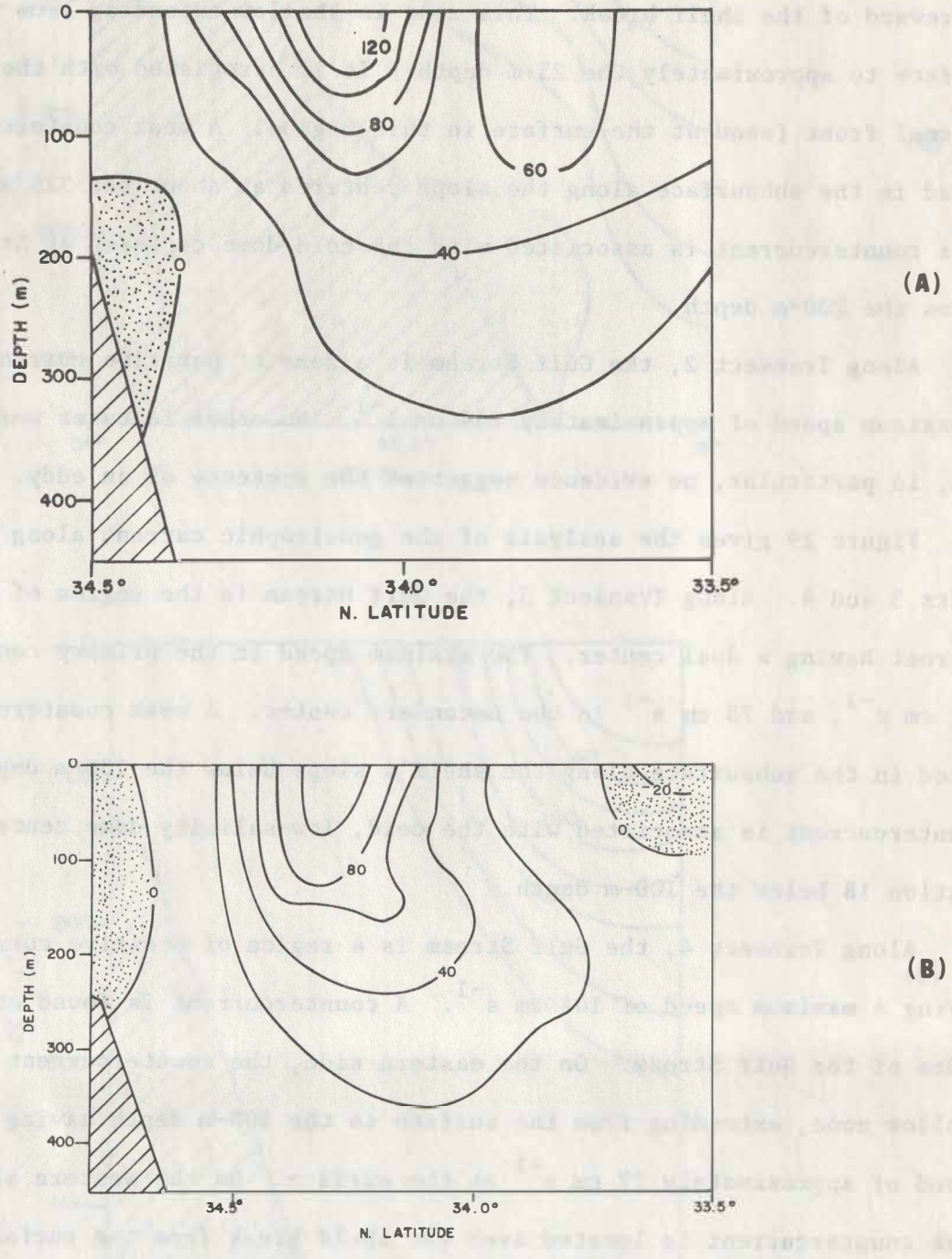

Figure 29. Analysis of geostrophic current (cm s^{-1}) along Transects 3 and 4

dome centered at Station 15 below the 100-m depth. This is the only analysis that shows indications of the countercurrent at the surface, and it exists only because the vertical current shear between the 75-m depth, the level of maximum current, and the surface was not sufficient to produce a zero current or a positive current at the surface. Since the surface current speed (6 cm s^{-1}) is small and since the satellite data gave no indication of a countercurrent at the surface in this particular eddy, the reality of the surface manifestation of this countercurrent is dubious.

The analysis of the depth of the 21°C, the 17°C, the 13°C, and the 9°C isotherms using the data collected along the four transects is given in Figure 30. As indicated earlier, a spatial distribution of the depth of isotherms is correlated with the spatial distribution of the streamlines flow. The analysis shows indication of cyclonic motion only for the 13°C and the 9°C isotherms (below the 200-m depth) in a location consistant with that for the western boundary eddy of interest. There are also indications of the upstream eddy. The fact that the analysis for the 13°C isotherm has a closed contour at the 200-m depth and no other closed contours are indicated for the other isotherms, suggest that circulation is strongest at around the 200-m depth.

The indication of shoreward transport in the analysis of the 9°C and the 13°C isotherm in the downstream regions of the eddy detected in the satellite data could explain the high-salinity tongues found in the analysis of the salinity data collected along Transects 1, 3, and 4. In these cases, the transport would have to be isothermal since there were no temperature changes. However, the data also indicate that there would be offshore transport in locations coincident with Transect 2. The salinity analysis

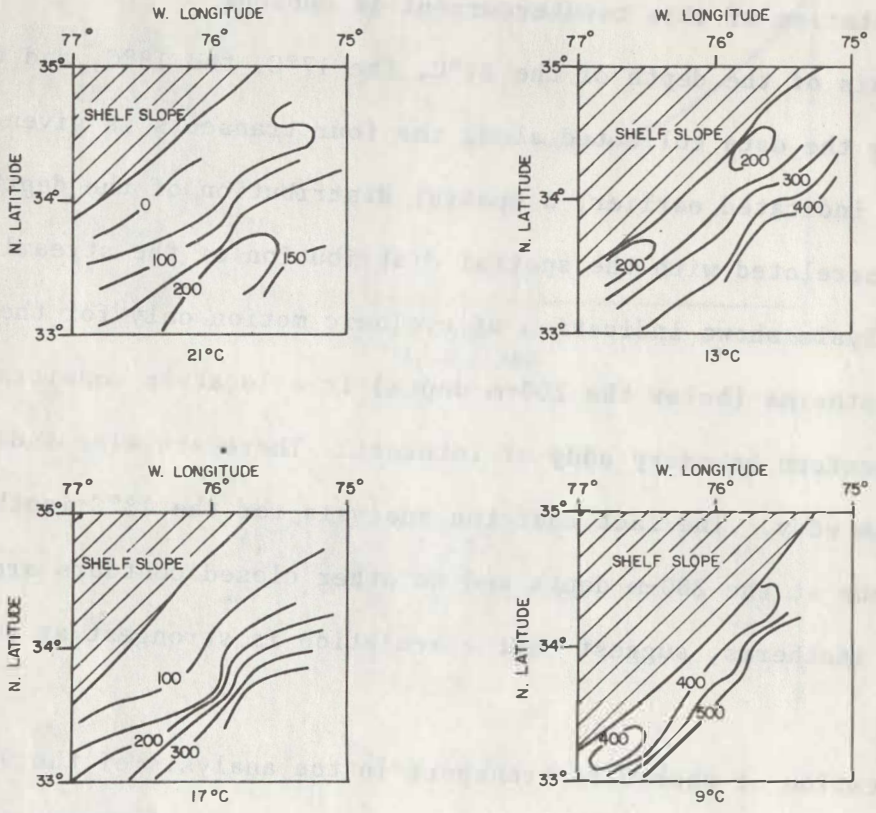

Figure 30. Analysis of the depth (m) of the 21° C, 17° C, 13° C, and 9° C isotherm using data from Transects 1 through 4

from data collected along Transect 2 also show weak indications of a high-salinity tongue. If the circulation is truly closed as indicated in the 13°C isotherm analysis, then it is possible that the tongue is being wrapped around the center of the eddy. A similar feature was noted in cyclonic rings located on the eastern side of the Gulf Stream (Vukovich and Crissman, 1978).

6.0 THEORETICAL DEVELOPMENT

6.1 Introduction

From the examination of available satellite imagery, it was noted that the western boundary eddy, which is the focal point of this study, developed immediately downstream of the Charleston Bump (centered at approximately 32.0°N and 79.0°W). A similar conclusion was drawn by Legeckis (1979). Though the theory for continental shelf waves indicates that perturbations can develop in the presence of a sloping shelf, wind stresses, and atmospheric pressure fluctuations (Robinson, 1964; Mysak, 1967; Caldwell, Cutchin, and Longuet-Higgins, 1972; and Magaard, 1977), the theories do not suggest any preferred location for the development of these perturbations. The fact that these perturbations have been observed to develop immediately downstream from the Charleston Bump suggests that the bump may be playing a significant role in the development. In this section, a simple, linear theory is developed to demonstrate the influence of a topographic feature similar to the Charleston Bump on the flow in the immediate vicinity and downstream of the feature. The results of the theory are then compared with the observational evidence presented in the previous sections.

6.2 Mathematical Development

An ocean is assumed which is infinitely long in the x-direction (west-east axis). In the y-direction (south-north axis), the ocean is of finite length defined by L_y (Figure 31). It is assumed to have a mean depth (D) and has a topographic bottom feature (H_B) similar to a hill (which is one way of characterizing the Charleston Bump). The exact specifications of the topographic feature will be given later in the mathematical development. It will also be assumed that the ocean has a mean current, $\bar{v}$, independent of

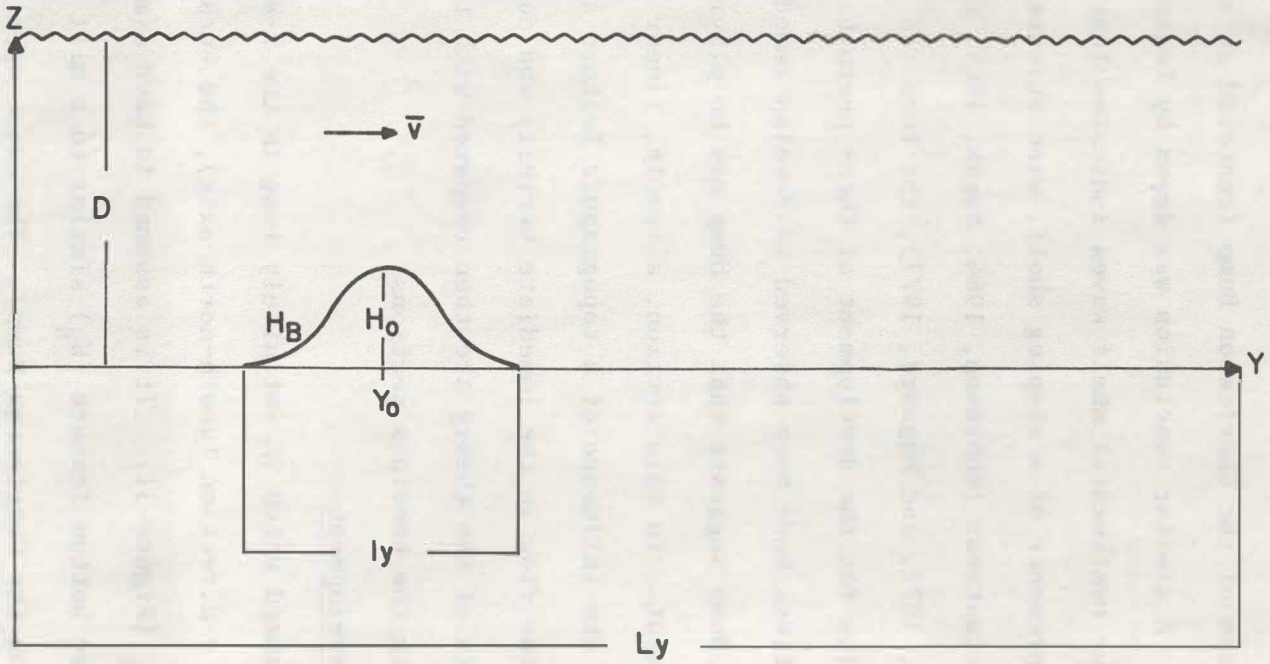

Figure 31. Geophysical description of parameters and domain of the model

time and space, and flowing in the positive y-direction (northward flow). In general, this characterizes the condition found off the southeast coast of the United States seaward from the shelf break.

The linearized perturbation vorticity equation characterizing the flow for the above specified conditions is:

$$\frac{\partial \zeta'}{\partial t} + \bar{v} \frac{\partial \zeta'}{\partial y} = -f D_H' \; ; \qquad (1)$$

where:

ζ' is the perturbation horizontal component of the vorticity,

f is the Coriolis parameter, and

D_H' is the perturbation horizontal component of the divergence.

In deriving equation (1), it was assumed that the equation for the mean horizontal component of the vorticity was

$$\frac{\partial \bar{\zeta}}{\partial t} + \bar{v} \frac{\partial \bar{\zeta}}{\partial y} = -\bar{v}\beta \; , \qquad (2)$$

where:

$\bar{\zeta}$ is the mean horizontal component of the vorticity,

β is the Rossby parameter.

It was also assumed that the perturbation Rossby term and the vertical advection of vorticity are negligible. The Rossby term was neglected because the scale of the perturbation is small so that the effect of the Coriolis force is negligible. The vertical advection term was neglected because vertical velocities are generally very small compared to horizontal velocities in the ocean. The principal forcing function in equation (1) is the divergence and convergence associated with the flow over the bottom feature.

Since the fluid is incompressible, the three-dimensional divergence is zero; i.e.,

$$\frac{\partial w'}{\partial z} = -D'_H \quad , \tag{3}$$

where w' is the perturbation vertical velocity.

Substitution of equation (3) into equation (1) yields,

$$\frac{\partial \zeta'}{\partial t} + \bar{v} \frac{\partial \zeta'}{\partial y} = f \frac{\partial w'}{\partial z} \quad . \tag{4}$$

Averaging equation (4) over depth yields the following expression:

$$\frac{\partial \zeta}{\partial t} + \bar{v} \frac{\partial \zeta}{\partial y} = \frac{f}{D} (w_o - w_B) \quad , \tag{5}$$

where:

$$\zeta = \int_{-D}^{o} \zeta' \, dz \Big/ \int_{-D}^{o} dz \quad , \tag{6}$$

w_o is the vertical velocity at the surface, and

w_B is the vertical velocity at the bottom.

It was assumed that the vertical velocity at the surface was zero ($w_o = 0$) and that the vertical velocity at the bottom can be given by the following expression:

$$w_B = \bar{v} \frac{\partial H_B}{\partial y} \quad . \tag{7}$$

Substitutions yielded:

$$\frac{\partial \zeta}{\partial t} + \bar{v} \frac{\partial \zeta}{\partial y} = - \frac{\bar{v} f}{D} \frac{\partial H_B}{\partial y} \quad . \tag{8}$$

It was next assumed that the bottom feature, H_B, is Gaussian in shape (Figure 31), and, therefore, can be given by the following expression:

$$H_B (y) = H_o \exp \left[-b^2 (y - y_o)^2 \right] , \tag{9}$$

where:

b^2 is the rate constant and is proportional to the scale length, l_y, of the bottom feature (see Figure 31),

H_o is the amplitude of the bottom feature, and

y_o is the location of the center of the bottom feature.

It was then assumed that a Fourier series exists which can be used to represent equation (9); i.e.,

$$H_B(y) = H_o \exp\left[-b^2(y-y_o)^2\right] = \sum_{n=0}^{\infty} a(k) \sin ky + b(k) \cos ky \quad , \qquad (10)$$

where:

$$a(k) = \frac{2}{L_y} \int_o^{L_y} H_B(y) \sin ky \, dy \text{ and } b(k) = \frac{2}{L_y} \int_o^{L_y} H_B(y) \cos ky \, dy \quad , \qquad (11)$$

and $k = 2\pi n/l_y$ where $n = 0, 1, 2, 3, \ldots, \infty$.

Under these conditions, the solution to equation (8) is

$$\zeta = \sum_{n=0}^{\infty} r(t,k) \sin ky + g(t,k) \cos ky \quad , \qquad (12)$$

provided

$$\begin{aligned} \frac{\partial r}{\partial t} - k \bar{v} g &= \frac{\bar{v} k f}{D} b(k) \quad , \\ \frac{\partial g}{\partial t} + k \bar{v} r &= -\frac{\bar{v} k f}{D} a(k) \quad . \end{aligned} \qquad (13)$$

Simultaneous solution of equation (13) yields

$$\begin{aligned} \frac{\partial^2 r}{\partial t^2} + \omega^2 r &= \frac{-\omega^2 f}{D} a(k) \quad , \\ \frac{\partial^2 g}{\partial t^2} + \omega^2 g &= \frac{-\omega^2 f}{D} b(k) \quad , \end{aligned} \qquad (14)$$

where:

$$\omega^2 = \bar{v}^2 k^2 \quad . \qquad (15)$$

The solution to equation (14) was subject to the following boundary conditions.

$$\zeta' = \zeta = 0, \; t = 0 \; ; \text{ or}$$
$$g = r = 0, \; t = 0 \; . \tag{16}$$

The boundary equations in equation (16) were substituted into equation (13) to yield two additional boundary conditions needed to solve equation (14); i.e.,

$$\left.\begin{aligned} \frac{\partial r}{\partial t} &= \frac{\omega f}{D} \, b(k) \\ \frac{\partial g}{\partial t} &= \frac{-\omega f}{D} \, a(k) \end{aligned}\right\} \quad , \; t = 0 \; . \tag{17}$$

When the boundary conditions in equations (16) and (17) are applied, the solution to equation (14) is

$$\begin{aligned} r(t,k) &= -\frac{f}{D} \, a(k) \, (1-\cos \omega t) + \frac{f}{D} \, b(k) \sin \omega t \; , \\ g(t,k) &= -\frac{f}{D} \, b(k) \, (1-\cos \omega t) - \frac{f}{D} \, a(k) \sin \omega t \; . \end{aligned} \tag{18}$$

Substitution of equation (18) into equation (12) yields the expression for the depth-integrated perturbation horizontal component of the vorticity associated with flow over a bottom feature similar to the Charleston Bump; i.e.,

$$\zeta = \frac{f}{D} \sum_{n=0}^{\infty} A(k) \, [\cos \{ k(y-\bar{v}t)-\phi \} - \cos (ky-\phi)] \tag{19}$$

where:

$$A^2(k) = a^2(k) + b^2(k) \text{ and } \phi(k) = \tan^{-1} \frac{a(k)}{b(k)} \; . \tag{20}$$

From equation (19), it is seen that the depth-integrated perturbation horizontal component of the vorticity is directly proportional to the ratio of the local Coriolis parameter and the local depth. As the depth of the ocean increases, the intensity of the perturbation decreases.

The solution is made up of two components: a forced response and a transient response. The forced response is a region of anticyclonic vorticity fixed in space centered about the bottom feature. This portion of the solution corresponds well with the persistent anticyclonic deflection noted at the Charleston Bump by Legeckis (1979).

The transient response is a region of cyclonic vorticity which moves downstream at a speed governed by the mean current. Computations made in Section 5.0 of the geostrophic current near the shelf break (200-m isobath) indicate speeds on the order of 20 to 40 km day^{-1}. It was noted in Section 3.0 that the average speed of the perturbations observed in the satellite data was either 24 km day^{-1} or 31 km day^{-1} depending on the location of the perturbations relative to the bump.

The theory indicates that the scale of both the forced and transient response is identical to the scale of the topographic feature (l_y). The scale for the Charleston Bump is approximately 150 km ± 20 km (the Charleston Bump does not approximate a Gaussian hill, but for the sake of argument, a Gaussian approximation was made). It is noted that the average wavelength of the eddies found immediately downstream of the Charleston Bump was approximately 148 km (see Section 3.0) and that, in the case study in Section 4.0 of a developing western boundary eddy, the steady-state wavelength was 160 km. Legeckis (1979) found an average wavelength of 150 km.

Figure 32 presents the results using equation (19) to determine the perturbation horizontal vorticity distribution in the first 5 days. For the computations, the average current was assumed to be 24 km day^{-1} ($\bar{v}$ = 24 km day^{-1}), the average depth was assumed to be 600 m (D = 600 m), the amplitude of the bottom feature was assumed to be 200 m (H_o = 200 m), the scale length

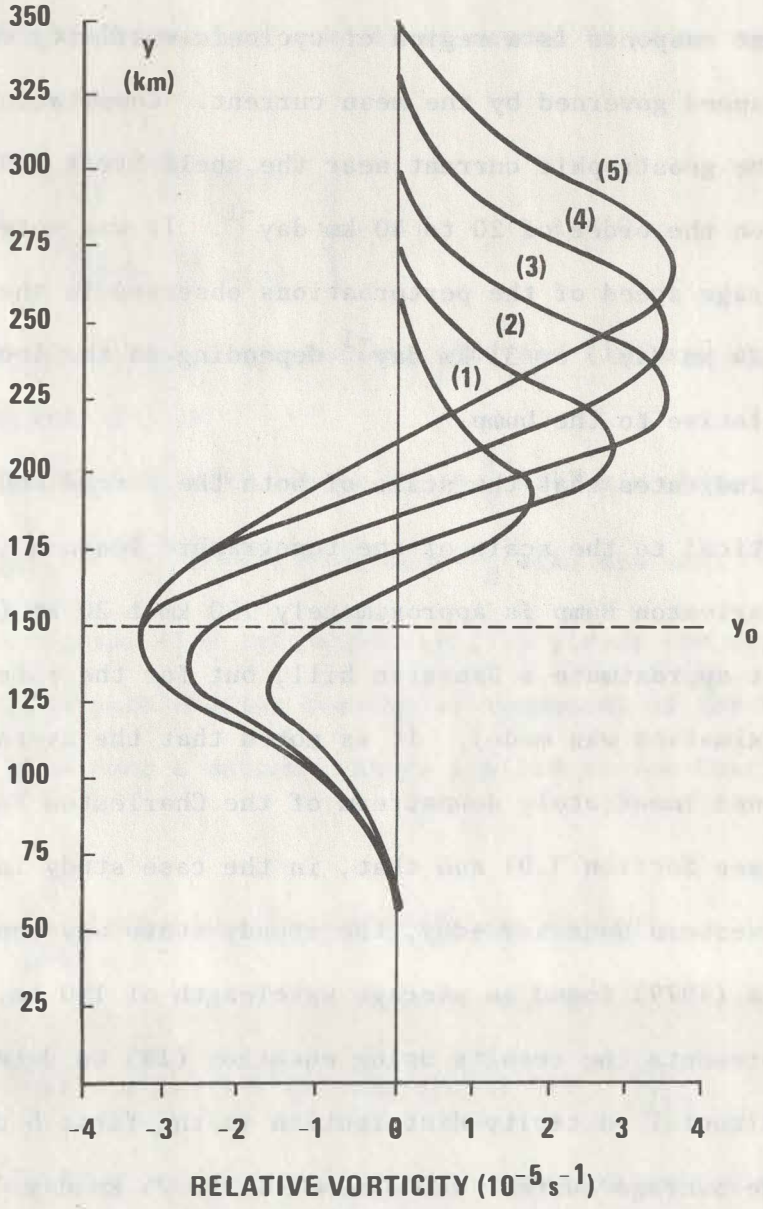

Figure 32. Solution for the vorticity (s^{-1}) distribution for the forced and transient response in the first 5 days (see text for model parameters)

of the bottom feature was 150 km (l_y = 150 km), the bottom feature was centered at y = 150 km (i.e., y_o = 150 km), and the mean latitude was assumed to be 33°N.

The computations showed that an anticyclonic perturbation developed upstream from the center of the bottom feature, and a cyclonic perturbation developed immediately downstream. Both perturbations progressed downstream. After 3 days, both perturbations reached their peak development, the anticyclonic perturbations became stationary over the center of the bottom feature, but the cyclonic perturbation continued moving downstream. It is not until after the third day that the motion of the cyclonic perturbation is directly related to the speed of the mean current.

The theoretical results describing the downstream development of the cyclonic vorticity is in qualitative agreement with the description of the development of the western boundary eddy in Section 4.0. The eddy was first detected about 83 km downstream of the bump and had an average speed between the night of 10 April and the morning of 13 April of approximately 34 km day^{-1} (i.e., the average speed over the two-and-one-half day period is probably a more reliable estimate of the wave speed than the wave speeds computed over the one-half-day periods given in Table 2). In the theoretical results, the cyclonic vorticity was first detected about 50 km downstream of the bump, and the mean current speed was 24 km day^{-1}. If a mean current of 34 km day^{-1} were used instead, the theoretical calculations would have been more in keeping with what was observed. The eddy in the case study also reached a steady state in 3 days. Without the influence of other forces, the theoretical calculations indicated that the cyclonic perturbation would continue downstream in an undisturbed manner (Figure 33).

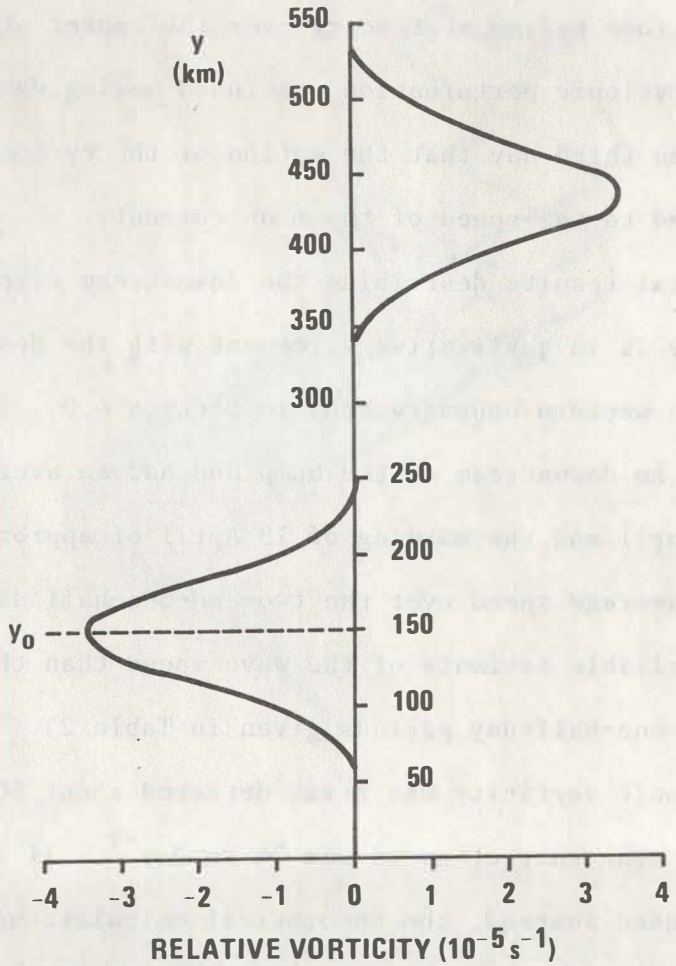

Figure 33. Vorticity (s^{-1}) distribution for the forced and transient response after 12 days

6.3 The Effect of Friction

Since the results in Section 3.0 suggested that the western boundary eddies weaken as they move downstream, it was decided to extend this theory by adding a linear friction term to the equation of motion. Under this condition, the linearized perturbation vorticity equation characterizing the flow is

$$\left(\frac{\partial}{\partial t} + K\right)\zeta' + \bar{v}\frac{\partial \zeta'}{\partial y} = -f D_H' \quad , \tag{21}$$

where K is the linear friction coefficient and is independent of time and space. Following the procedures outlined in equations (3)-(11) in Section 6.2, equation (12) is the solution provided

$$\begin{aligned}\left(\frac{\partial}{\partial t} + K\right) r - k\bar{v}g &= \frac{\bar{v}kf}{D} b(k) \quad , \\ \left(\frac{\partial}{\partial t} + K\right) g + k\bar{v}r &= \frac{-\bar{v}kf}{D} a(k) \quad .\end{aligned} \tag{22}$$

Simultaneous solution of equation (22) yields the following expression:

$$\begin{aligned}\left(\frac{\partial^2}{\partial t^2} + 2K\frac{\partial}{\partial t} + \omega_o^2\right) r &= M_1 \quad , \\ \left(\frac{\partial^2}{\partial t^2} + 2K\frac{\partial}{\partial t} + \omega_o^2\right) g &= M_2 \quad ;\end{aligned} \tag{23}$$

where

$$\begin{aligned}\omega_o^2 &= \bar{v}^2k^2 + K^2 \quad , \\ M_1 &= \frac{-\omega^2 f}{D}a(k) + \frac{\omega k f}{D}b(k) \quad , \\ M_2 &= \frac{-\omega^2 f}{D}b(K) - \frac{\omega k f}{D}a(k) \quad .\end{aligned} \tag{24}$$

When the boundary conditions in equations (16) and (17) are applied, the solution to equation (23) under the conditions that $\omega > K$ is

$$r(t,k) = \frac{M_1}{\omega_o^2}\left[1 - \frac{\omega_o}{\omega}e^{-Kt}\sin(\omega t + \lambda)\right] + \frac{f}{D}\,b(k)e^{-Kt}\sin\omega t\,,$$

$$g(t,k) = \frac{M_2}{\omega_o^2}\left[1 - \frac{\omega_o}{\omega}e^{-Kt}\sin(\omega t + \lambda)\right] - \frac{f}{D}\,a(k)e^{-Kt}\sin\omega t\,; \tag{25}$$

where

$$\lambda = \tan^{-1}\left(\frac{\omega}{K}\right). \tag{26}$$

Substitution of equation (25) into equation (12) yields the solution for the depth-integrated perturbation horizontal component of the vorticity with friction included; i.e.,

$$\zeta = \frac{f}{D}\sum_{n=0}^{\infty} A(k)\left[e^{-Kt}\cos\left\{k(y - \bar{v}t) - \phi + \lambda_o\right\} - \cos(ky - \phi + \lambda_o)\right], \tag{27}$$

where

$$\lambda_o = \tan^{-1}\left(\frac{K}{\omega}\right). \tag{28}$$

According to the expression in equation (27), there are two effects of frictional processes. The transient response is damped with time, and the forced response is displaced upstream from the bottom feature. The upstream displacement of the forced response is dependent on the magnitude of the linear friction term (see equation (28)). The maximum possible value of the argument of the arctangent in equation (28) cannot equal or exceed unity since a condition for the solution presented is that $\omega > K$.

Figure 34 shows the solution for the transient cyclonic perturbation after 12 days for the parameter values given in Section 6.2 and for the various values of the linear friction coefficient. Upstream displacements

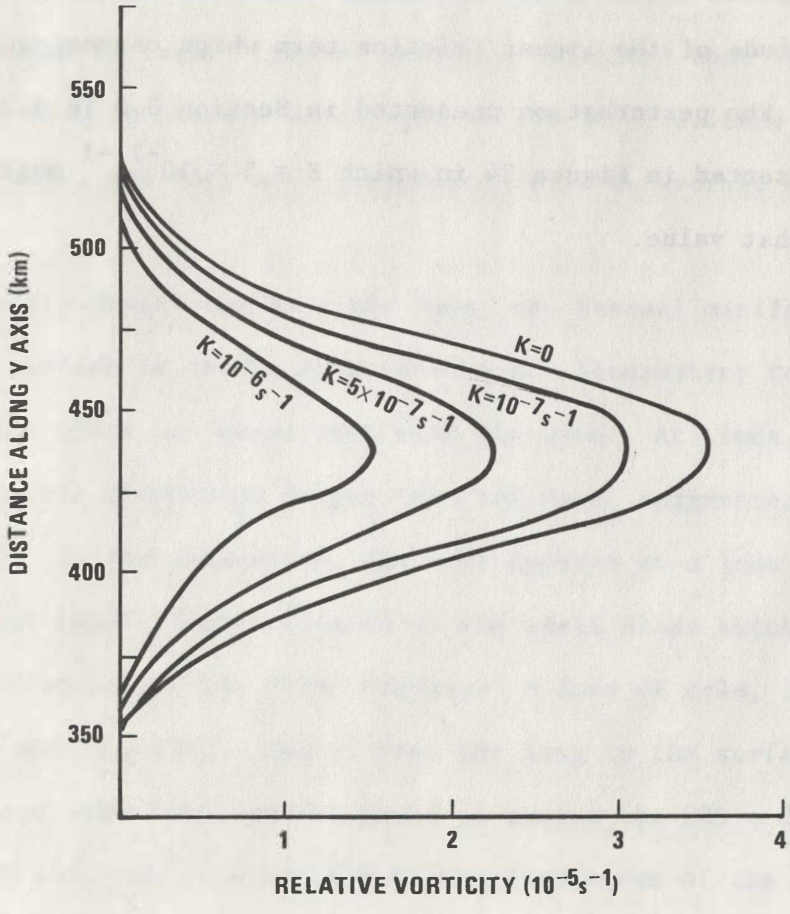

Figure 34. Vorticity (s^{-1}) distribution for the transient response after 12 days using various values of the linear friction coefficient (s^{-1}).

of the forced response were negligible (e.g., for the case when $K = 10^{-6} s^{-1}$, the displacement was on the order of 5 km).

Using the mean amplitude data presented in Section 3.0, assuming an exponential decay of the perturbation, a mean speed for the perturbation of 24 km day^{-1}, and a travel distance of 288 km in 12 days (the approximate distance between the center of the Charleston Bump and the 34°N latitude line), the magnitude of the linear friction term which corresponds to the average decay of the perturbation presented in Section 3.0 is $4.2 \times 10^{-7} s^{-1}$. The solution presented in Figure 34 in which $K = 5 \times 10^{-7} s^{-1}$ most closely corresponds to that value.

7.0 DISCUSSION OF RESULTS

The results of this study suggest that a class of Gulf Stream western boundary eddies develop immediately downstream from the Charleston Bump (within 100 km), which is centered at about 32°N and 79°W. In this region, the bottom topography is influenced by the Blake Plateau. The dimensions (wavelength and amplitude) of eddies reached a steady state within 2 to 3 days after they began to form. Limited analysis indicated that after formation these eddies have an average wavelength of 148 km, amplitude of 52 km, and period of 6 days; and they move northeastward at an average speed of 24 km day^{-1}.

Immediately downstream from the bump, the thermal manifestation of the eddy at the surface is in the form of a wave. Alternating tongues of cold and warm water often are associated with the wave. At times, the warm and cold tongues have dimensions larger than the wave, suggesting a very complex perturbation. In the subsurface, the eddy appears as a lens of cold, low-salinity, high-density water located on the shelf slope which is not steep due to the influence of the Blake Plateau. A dome of cold, low-salinity, high-density water projects upward from the lens to the surface. The case study indicated that the lens was found at around the 325-m depth, and the dimensions of the lens were similar to the dimensions of the thermal wave at the surface. The data also indicated that the lens moved upward along the shelf slope. The calculated upward speed was 0.1 mm s^{-1}.

The *in situ* and satellite data indicated intense cyclonic motion associated with the eddy from the surface to the 300-m depth. This is supported by the following factors. A countercurrent, relative to the Gulf Stream current, was located over the shelf break on the shoreward side of the eddy, and extended from the surface to about the 175-m depth. The counterflow

was associated with the warm tongue. Immediately downstream from the crest of the thermal wave, the *in situ* data indicated subsurface shoreward motions. In this same region, there was a tongue of high salinity extending from the high-salinity core of the Gulf Stream, suggesting transport by the eddy motions. The geostrophic current speeds were a maximum in the Gulf Stream near the crest of the thermal wave. This is believed to be a result of density gradients (current) associated with the eddy augmenting the density gradients (current) associated with the Gulf Stream.

When the eddies move north of 34°N where the bottom topography is no longer affected by the Blake Plateau, the dimensions of the eddy decrease. In this region, the average wavelength was 115 km and the amplitude was 34 km. The average wave speed increased (31 km day^{-1}), but the wave continued to move northeastward. The average period was about 4 days. The wave speeds may be larger far downstream because these waves, at times, become stationary in their formative stages immediately downstream from the bump.

At the surface, the thermal manifestation of the eddy was in the form of a wave. An interesting feature noted in the satellite data was a cold lens within the eddy displaced downstream from the crest of the wave. This feature persisted for at least 5 days in a region where free-drifting buoy data and other *in situ* data indicated there were significant currents. These currents should have quickly mixed the cold water in the lens with the surrounding environment. The fact that the feature persisted suggested that the lens may be sustained by an upwelling process.

In the subsurface, the eddy was a dome of cold, low-salinity, high-density water located immediately seaward of the slope, which was very steep,

being in a region no longer influenced by the Blake Plateau. The dome was found below the 100-m depth and exceeded the 500-m depth. Cyclonic motion was again evident; but the counterflow on the shoreward side was found at depth, reaching the surface only in the downstream portions of the eddy. There was evidence of shoreward motion immediately downstream from the center of the eddy; and as in the case of the eddy immediately downstream from the bump, a high-salinity tongue extended shoreward from the high-salinity core of the Gulf Stream, suggesting transport by the currents associated with the eddy. Maximum surface geostrophic currents were noted near the crest of the wave. In this case, data from surface drifters supported the notion that surface current speeds increased through the eddy. Overall, there were significant differences in the structure of eddies found immediately downstream from the bump and those found far downstream, suggesting that the eddy decreased in intensity as it moved downstream.

The results of a theoretical study suggests that eddies may be developed by the convergence and divergence pattern associated with flow over a topographical feature similar to the Charleston Bump (lee waves). The solution produced a forced responsed, a region of anticyclonic vorticity, centered over the topographic feature. This compared well with the anticyclonic deflection of the Gulf Stream western boundary at the Charleston Bump noted by Legeckis (1979). A transient response, a zone of cyclonic vorticity, develops immediately downstream of the feature (within 50 to 100 km), a factor that corresponds with observed data. Both the forced and transient response have a wavelength comparable to the scale of the topographic feature. The scale of the Charleston Bump is on the order of 150 km ± 20 km. It is noted that the average wavelength of the eddies observed immediately down-

stream from the bump was 148 km, and that Legeckis found an average wavelength of 150 km for these features. The transient response reaches a steady state in 3 days, also consistent with observed data. In theory, the transient response moves downstream at a speed identical to a depth-integrated current speed. According to the geostrophic computations, the depth-integrated currents in the vicinity of the shelf break varied from 20 to 40 km day^{-1}. The satellite data indicated that the average speed for the eddies immediately downstream of the bump was 24 km day^{-1}, and was 31 km day^{-1} for those far downstream.

The theoretical results indicate that the intensity of the eddy decreases with increasing depth of the ocean or by frictional dissipation. The data analysis showed that the most intense eddies were observed where the slope was relatively flat due to the influence of the Blake Plateau. The flat slope allowed the eddy to affect approximately the first 300 m only. When the eddy moved farther downstream, it was located in a region no longer affected by the Blake Plateau and the local bottom depth exceeded 1000 m. In this region, the eddy was observed to be less intense than that found farther downstream. If frictional forces were responsible for the change in the eddies, an average linear friction coefficient on the order of 5×10^{-7} s^{-1} would be required. The observed data were not sufficient to discriminate which of these factors predominated, if any.

The theoretical model simplifies the physics of the western boundary eddies, but does explain some of the more rudimentary factors associated with these eddies. It does not explain the recurrence of the eddies, nor does it explain the unstable modes discussed by Legeckis. During the course of this study, it was noted that many of these eddies appeared to develop shortly

after a frontal passage, suggesting that this condition allows the flow parameters of the Gulf Stream to re-initialize, which is similar to what occurs in the case of atmospheric lee waves. Furthermore, since these waves develop in the presence of both horizontal and vertical current shear associated with the Gulf Stream, unstable modes can be created by either baratropic or baroclinic forces, or both. However, until more comprehensive analyses are performed, these factors remain mere conjecture.

8.0 REFERENCES

Brooks, D.A., 1975: Wind-forced continental shelf waves in the Florida Current, Ph.D. thesis, University of Miami.

Caldwell, D. R., D. L. Cutchin, and M. S. Longuet-Higgins, 1972: Some model experiments on continental shelf waves. J. Marine Res., 30, 3955.

DeRycke, R. J., and P. K. Rao, 1973: Eddies along a Gulf Stream boundary from a very high resolution radiometer, J. Phys. Oceanogr., 3, 490-492.

Kunde, V. G., 1965: Theoretical relationship between the equivalent blackbody temperature and surface temperature measured by the NIMBUS high resolution infrared radiometer. In: Observations from the NIMBUS-I Meteorological Satellite, NASA SP-89, 23-26.

Legeckis, R. V., 1979: Satellite observation of the influence of bottom topography on the seaward deflection of the Gulf Stream off Charleston, South Carolina. To be published in J. Phys. Oceanogr., 9:3 1979.

Magaard, L., 1977: On the generation of baroclinic Rossby waves in the ocean by meteorological forces. J. Phys. Oceanogr., 7, 359-364.

Mysak, L. A., 1967: On the theory of continental shelf waves. J. Marine Res., 25, 205-227.

Mysak, L. A., and B. V. Hamon, 1969: Low-frequency sea level behavior and continental shelf waves off North Carolina. J. Geophys. Res., 74, 1397-1404.

Niiler, P. P., and L. A. Mysak, 1971: Barotrophic waves along an eastern continental shelf, Geophys. Fluid Dyn., 2, 273-288.

NIMBUS-6 Users Guide, 1975: prepared by the LANDSAT-1 NIMBUS Project GSFS, NASA. Edited by J. E. Sissala. 263 pp.

Orlanski, I., 1969: The influence of bottom topography on the stability of jets in a baroclinic fluid. J. Atmos. Sci., 26, 1216-1232.

Rao, P. K., A. E. Strong, and R. Koffler, 1971: Gulf Stream meanders and eddies as seen in satellite infrared imagery, J. Phys. Oceanogr., 237-239.

Richardson, P. L., and J. A. Knauss, 1971: Gulf Stream and western boundary undercurrent observations at Cape Hatteras, Deep Sea Res., 18, 189-1109.

Robinson, A. E., 1964: Continental shelf waves and the response of the sea level to weather systems. J. Geophys. Res., 69, 367-368.

Schott, F., and W. Düing, 1976: Continental shelf waves in the Florida shelf. J. Phys. Oceanogr., 6, 451-460.

Smith, W. L., P. K. Rao, R. Koffler, and W. R. Curtis, 1970: The determination of sea surface temperatures from satellite high resolution infrared window radiation measurements, Mon. Weather Rev., 98(8), 607-611.

Stumpf, H. G., and P. K. Rao, 1975: Evolution of Gulf Stream eddies as seen in satellite infrared imagery, J. Phys. Oceanogr., 5, 388-393.

Vukovich, Fred M., and Bobby W. Crissman, 1977: Study of oceanic processes of the east coast of the United States using data from a NOAA satellite and from a surface vessel. Final report, NOAA contract No. 6-35263, Research Triangle Institute, Research Triangle Park, N.C., 76 pp.

Vukovich, Fred M., and Jackson O. Blanton, 1969: Physical oceanography feasibility study utilizing NIMBUS 2 HRIR satellite data, Final Report, ESSA Contract No. E-256-68(N), Research Triangle Institute, Research Triangle Park, N.C., 133 pp.

Vukovich, F. M., 1972: Synoptic-scale air-sea interaction study using NOAA-1 SRIR data. Final Report, NOAA Contract No. 2-35184, Research Triangle Institute, Research Triangle Park, N.C., 85 pp.

Vukovich, F. M., 1976: An investigation of a cold eddy on the eastern side of the Gulf Stream using NOAA 2 and NOAA 3 satellite data and ship data, J. Phys. Oceanogr., 6, 605-612.

Vukovich, F. M., and B. W. Crissman. 1975: Case study of exchange processes on the western boundary of the Gulf Stream using NOAA-2 satellite data and ship data. Remote Sens. Environ., 4, 165-176.

Vukovich, F. M., and B. W. Crissman. 1978: Further studies of a cold eddy on the eastern side of the Gulf Stream using satellite data and ship data. J. Phys. Oceanogr., 8:5, 838-845.